IN VIVO AND EX VIVO MRI STUDIES OF AN ANIMAL MODEL OF MESIAL TEMPORAL LOBE EPILEPSY CORRELATED WITH HISTOLOGICAL ANALYSIS

By

LAN HOANG MINH

A THESIS PRESENTED TO THE GRADUATE SCHOOL
OF THE UNIVERSITY OF FLORIDA IN PARTIAL FULFILLMENT
OF THE REQUIREMENTS FOR THE DEGREE OF
MASTER OF SCIENCE

UNIVERSITY OF FLORIDA

2008

© 2008 Lan Hoang Minh

To my family and friends for their love and encouragement.

ACKNOWLEDGEMENTS

First, I would like to thank my committee members, Drs. Thomas Mareci, Paul Carney and Steve Blackband for their guidance and encouragement. I would like to thank my mentor, Dr. Mareci, for his continuous support and for shaping my knowledge of MR imaging, as well as teaching me how to operate the magnet systems; Dr. Carney, for providing his expertise on epilepsy and guiding the project by emphasizing the clinical relevance of our research; Dr. Blackband, for providing me a foundation on the basic principles of MR imaging. I would also like to thank Dr. Michael King for his help with histology experiments.

I am indebted to all of the current and former members of the Mareci and Carney labs that I have had the opportunity to work with over the past two years. In particular, I would like to thank my lab mate, Hector Sepulveda for building the surface coils, the stereotaxic frame and helping with MR imaging data acquisition; Mansi Parekh for contributing to MR imaging data acquisition and some of the histology experiments; Dr. Wendy Norman, for taking care of the animals and monitoring them over the entire course of *in vivo* imaging; Angela Hadlock, for performing the surgical implantation of electrodes; Chad Durgin, for improving the data analysis software; and Jessica Meloy and Matthew Feldman for providing assistance in data analysis. I also appreciate other current and former lab members, Garrett Astary, Nelly Volland, Chris Taylor, Min Sig Hwang, for their help and moral support.

I would like to give credit to the Advanced Magnetic Resonance Imaging and Spectroscopy (AMRIS) facility and staff at the McKnight Brain Institute of the University of Florida. I thank Xeve Silver and Gary Blaskowski for technical support with the magnet systems; Barbara Beck and Kelly Jenkins, for their expertise in coil setup and design; and Jim Rocca and Dan Plant for making sure that all the machines were running properly. I am also grateful for the

financial support provided by the University of Florida Alumni Foundation, the McKnight Brain Institute, Wilder Epilepsy Research Center and National Institutes of Health.

I would also like to thank my family in France and in the United States for their continuous love, support and encouragement throughout the years; my friends in Gainesville, especially Berenger, for their moral support, particularly during the last months while finishing my experiments and writing my thesis.

TABLE OF CONTENTS

LIST OF FIGURES

Abstract of Thesis Presented to the Graduate School
of the University of Florida in Partial Fulfillment of the
Requirements for the Degree of Master of Science

IN VIVO AND EX VIVO MRI STUDIES OF AN ANIMAL MODEL OF MESIAL TEMPORAL LOBE EPILEPSY CORRELATED WITH HISTOLOGICAL ANALYSIS

By

Lan Hoang Minh

May 2008

Chair: Thomas Mareci
Major: Biomedical Engineering

Epilepsy is one of the most common neurological conditions worldwide and a significant cause of morbidity in modern society, especially in children and young adults. Mesial temporal lobe epilepsy (MTLE) is the most common form of symptomatic localization-related human epilepsy and the most common epilepsy syndrome with pharmacologically intractable partial-onset seizures. Patients often have an initial precipitating injury during early childhood, followed by a latent period of up to several years before the emergence of complex partial seizures. Understanding the mechanisms involved during epileptogenesis as well as the consequences of initial injuries is crucial in the diagnosis of epilepsy and development of effective strategies for therapeutic intervention.

Whether seizures cause permanent damage to the brain and lead to an epileptic lesion resulting in long-term epilepsy is a subject of controversy. Several cross-sectional magnetic resonance imaging (MRI) and histology studies have reported changes suggestive of seizure-associated damage in animal models. Very few longitudinal studies have been performed to describe acute seizure-associated changes and their evolution over time. Since epileptic conditions in humans develop over long periods of time and have effects extending over many years, clinical studies seeking the causes and mechanisms underlying the development of

epilepsy are very difficult and expensive to perform. Animal models allow for experiments that investigate the full dynamic course of the epileptic state. *In vivo* MRI permits the non-invasive detection of structural alterations in living animals, the dynamics of involvement and interactions between all the brain regions, as well as their progression in a single individual over the entire time-course of the disease.

The animal model of chronic limbic epilepsy used in this study is characterized by recurrent spontaneous hippocampal seizures following an episode of status epilepticus (SE) induced by a period of electrical hippocampal stimulation. Spontaneous seizures begin several weeks later and physiologically resemble seizures seen in human MTLE. High-resolution *in vivo* MRI was used to evaluate the progression of brain pathological alterations in the same animal at different time points, followed by *ex vivo* MRI, three-dimensional magnetic resonance microscopy at high field strength and histological analysis. The findings demonstrated that development of seizures was associated with significant changes in relaxation measurements following SE in the hippocampus, lateral ventricle regions, thalamus and parahippocampal gyrus, visible or not as changes in signal intensity on T1 or T2-weighted *in vivo* MRI images. These *in vivo* changes were due to underlying pathological tissue alterations evident with *ex vivo* MRI and histology, including iron deposition, neuronal degeneration and microglia aggregation.

Correlation of longitudinal *in vivo* imaging data with behavioral observations and post-mortem *ex vivo* MRI and histopathological analysis can help provide a more complete understanding of the causes and mechanisms underlying epileptogenesis. Continued improvement and application of these MRI techniques, particularly the development of diffusion-weighted and diffusion tensor imaging, will allow additional insights into the mechanisms involved in the epileptogenic process.

CHAPTER 1
INTRODUCTION

Mesial Temporal Lobe Epilepsy

Overview

Epilepsy is a chronic pathologic condition of the nervous system characterized by recurrent epileptic seizures. It is one of the most common neurological conditions, affecting at least 50 million people worldwide (Loscher and Ebert 1996), with an incidence rate of about 50 per 100,000 in developed countries (Sander 2003). It is a significant cause of morbidity in modern society, affecting mostly children and young adults (Sundqvist 2002). The various types of epilepsy are characterized by simultaneous activation of a large population of neurons resulting in abnormal electrographic and/or behavioral seizure activity (Pitkanen, et al. 2002).

Mesial temporal lobe epilepsy (MTLE) is the most common form of symptomatic (secondary) localization-related human epilepsy and the most common epilepsy syndrome with pharmacologically intractable partial-onset seizures (Cavazos and Cross 2006). It affects 20% of patients with epilepsy, with a cost of approximately $5 billion in the United States. MTLE is characterized by seizures arising from the hippocampus, parahippocampal gyrus and amygdala. Patients often have an initial precipitating injury during early childhood, such as status epilepticus, complicated febrile seizures, head trauma, etc., followed by a latent period of up to several years during which neurobiological changes take place that eventually lead to the onset of spontaneous seizures (Berg, et al. 1999, Knudsen and Auk 2000, Mathern, et al. 1997).

Status epilepticus (SE) has been defined as a seizure that shows no clinical signs of arresting after a duration encompassing the great majority of seizures of that type (usually 30 minutes), or recurrent seizures without interictal resumption of baseline central nervous system function (Blume, et al. 2001). SE can lead to the onset of chronic spontaneous seizures after a

latent period of epileptogenesis that can last several years. Understanding the mechanisms involved during epileptogenesis as well as the consequences of initial injuries is crucial in the diagnosis of epilepsy and the development of effective strategies for therapeutic intervention.

Pathophysiology

The syndrome of MTLE is the most common form of symptomatic localization-related epilepsy, due to a localized structural brain lesion, and is characterized by epileptogenic abnormalities in mesial temporal limbic structures (Engel 2001). Epileptic seizures arise from synchronous and sustained discharges from groups of neurons. Seizure discharges in MTLE patients initiate from mesial limbic structures such as the hippocampus, entorhinal cortex and amygdala (Bartolomei, et al. 2001, Blumenfeld, et al. 2004, Maillard, et al. 2004). This hyperexcitability may arise due to a number of different reasons that remain only partially understood (Liu, et al. 1995). These mesial limbic areas display the most prominent morphological changes.

The most prominent pathological manifestation associated with MTLE is usually hippocampal sclerosis (Figure 1-1) (Blumcke, et al. 1999, Liu, Mikati and Holmes 1995, Mathern, et al. 1996), as part of a typical pattern of brain damage in MTLE patients known as mesial temporal sclerosis (MTS) (Gloor 1997, Jackson, et al. 1998). However, other discrete structural lesions can also be found alone or in association with hippocampal sclerosis. Whether hippocampal sclerosis is a result of spontaneous seizures or causes seizure activity in the region is under debate.

The hallmark of MTS is a selective loss of neurons in the entorhinal cortex and the neighboring amygdala, in the dentate hilus, and in the CA3 and CA1 areas of the hippocampus. However, the granule cells of the dentate gyrus and the CA2 area of the hippocampus as well as the subiculum are relatively spared (Du, et al. 1993, Gloor 1997). The dense gliosis that

accompanies the loss of neurons causes shrinkage and hardening of tissue ("sclerosis"). Many studies have focused on the cell damage and consequent reorganization that characterize the dentate gyrus of MTLE patients. Normally, input to the hippocampus comes from the entorhinal cortex to the dentate granule cells through the perforant path (Chang and Lowenstein 2003). The dentate granule cells normally sprout mossy-fiber axons, which extend to CA3 pyramidal neurons as part of the hippocampal output pathway (Engel 2001). In hippocampal sclerosis, however, these cells sprout mossy-fiber axons that are directed back into the inner molecular layer (Babb, et al. 1991, Sutula, et al. 1989), possibly because the neurons to which they usually extend have been lost. These aberrant mossy fibers instigate a recurrent excitatory circuit by forming synapses on the dendrites of neighboring dentate granule cells. Excitation interneurons, which normally activate inhibitory interneurons acting on dentate granule cells, may be selectively lost, resulting in hyperexcitability (Sloviter 1991). Moreover, neurogenesis of new dentate granule cells was shown to be increased by seizures, and these neurons may integrate themselves into abnormal circuits (Parent, et al. 1997, Scharfman, et al. 2000).

In addition to morphological changes in the hippocampus, the most prominent changes at the molecular level were alterations in the composition and expression of inhibitory GABA receptors on the surface of hippocampal dentate granule cells, weeks before the onset of spontaneous seizures (Brooks-Kayal, et al. 1998). These altered receptors become highly sensitive to zinc released by mossy-fiber terminals after repetitive synaptic stimulation (during seizure initiation), leading to failure of inhibition (Buhl, et al. 1996). Some studies also suggest that neuronal injury following seizures may be mediated by an excitotoxic mechanism, with excessive excitability secondary to the release of excitatory amino-acids, primarily glutamate (Liu, et al. 1995).

In addition to the hippocampus, other mesiotemporal regions such as the entorhinal cortex, the amygdala and the piriform cortex (PC) have been associated with seizure generation (Bartolomei, et al. 2005, Bernasconi, et al. 1999, Bertram 1997, von Bohlen und, et al. 2004, Yilmazer-Hanke, et al. 2000). Studies have demonstrated the propagation of seizures from the entorhinal cortex to the CA1- subiculum region of the hippocampus through the temperoammonic pathway (Cossart, et al. 2001, Soltesz 1995, Wozny, et al. 2005). The PC sends projections to different limbic structures such as the entorhinal cortex as well as the periamygdaloid cortex and cortical amygdaloid nuclei (Goncalves, et al. 2005). It was shown to have a critical role in the generation of epileptogenic and ictogenic networks in experimental TLE (Bertram 1997, Loscher and Ebert 1996, McIntyre and Kelly 2000), and is associated with the development of spontaneous focal-onset seizures after SE (Roch, et al. 2002b).

The amygdala is heavily interconnected with the hippocampus and parahippocampal region and is prone to neuronal damage both in clinical and experimental TLE (Aliashkevich, et al. 2003, Hudson LP, et al. 1993, Kemppainen, et al. 2002, Tuunanen, et al. 1999). One of the major projections from the amygdala to the hippocampus terminates in the temporal aspect of the CA1/subiculum border region in rat (Pikkarainen, et al. 1999), which is affected in most patients with MTLE. The seizure activity that is initiated by the stimulation of the amygdala has been reported to cause secondary damage in the hippocampus. For example, loss of hilar neurons and sprouting of mossy fibers in the dentate gyrus occurred in rats that developed spontaneous seizures after a self-sustained status epilepticus was induced by electrical stimulation of the lateral nucleus of the amygdala (Pitkanen, et al. 2002). Stimulation studies demonstrate that action potentials are conducted from the amygdala to the entorhinal cortex in approximately 25 ms and from the amygdala to the temporal hippocampus in 20–40 ms (Buser and Bancaud 1983,

Wilson, et al. 1990), suggesting that several regions of the temporal lobe are readily recruited to participate in the seizure activity after its onset (Kemppainen and Pitkanen 2004). These data suggest a critical role for the entorhinal cortex, amygdala and PC in epileptogenesis as well as in the symptomatology of TLE, and suggest the necessity of looking at the dynamics of the entire limbic circuit when investigating the mechanisms of epileptogenesis.

Animal Model of Mesial Temporal Lobe Epilepsy

Animal models that reproduce the behavioral and neurophysiologic features of human epilepsy make them well suited for studying the causes and mechanisms underlying the development of epilepsy. They are particularly useful in studying the progressive changes over the entire time-course of the disease within a relatively short time frame, while those developments usually take several years in human patients. In animal models, the epileptogenic process has been initiated by chemically or electrically induced status epilepticus. However, in studies using systemically injected chemical convulsants such as pilocarpine or kainate (King, et al. 1991a, Niessen, et al. 2005), the mortality rates are high, and those models do not replicate the focal brain injury that usually initiates the epileptogenic process in human MTLE.

The rat chronic limbic epilepsy (CLE) model is a well-studied and accepted animal model of acquired TLE. CLE induced by hippocampal electrical stimulation is considered to be a model of epileptogenesis and spontaneous seizures provoked by an initial brain insult, and this model mimics many of the histopathologic characteristics of MTLE. Unilateral continuous electrical stimulation of the ventral hippocampus induces an episode of SE, followed by the onset of chronic epilepsy several weeks later (Bertram 1997, Bertram and Cornett 1994, Lothman, et al. 1989). In this model, neuronal loss and gliosis are seen throughout the limbic system and the thalamus, along with mossy fiber sprouting in the dentate hilus (Bertram and Lothman 1993, Bertram, et al. 1990, Bertram and Scott 2000), as seen in human MTLE patients. This model is

also refractory to anticonvulsant drugs, as is commonly seen in human MTLE. Moreover, the electrographic seizures resemble the seizures recorded in humans (Bertram and Cornett 1993, Bertram and Cornett 1994, Lothman, et al. 1990). The latent period lasting several weeks before the onset of spontaneous seizures makes it an ideal model to study epileptogenesis.

No studies to date have used MRI to investigate the epileptogenic and spontaneous seizure changes in this animal model of MTLE induced by hippocampal electrical stimulation. The similarities between the physiopathology in this model and the clinical pathology of human MTLE support the use of this animal model in the study of the mechanisms of epileptogenesis and epilepsy. Another advantage of this model is that it does not produce the mortality, morbidity and challenges that result from the use of systemic chemical convulsants.

In vivo Magnetic Resonance Imaging

Magnetic resonance imaging (MRI) has been the definitive modality for diagnosing most disorders of the central nervous system (CNS) over several years. MRI provides a key advantage in that it allows the noninvasive observation of many of the pathophysiological manifestations of CNS injury and disease, as well as their dynamic progression. Several cross-sectional magnetic resonance imaging (MRI) and histology studies have reported changes suggestive of seizure-associated damage in animal models. Very few longitudinal studies have been performed to describe acute seizure-associated changes and their evolution over time. Since epileptic conditions in humans develop over long periods of time and have effects extending over many years, clinical studies seeking the causes and mechanisms underlying the development of epilepsy are very difficult and expensive to perform.

In vivo MRI permits the non-invasive detection of structural alterations in living animal models of epilepsy, the dynamics of involvement and interactions between all the brain regions and their progression in a single individual over the entire time-course of the disease. When

living tissue is placed into a high static magnetic field, signal from hydrogen nuclei can be detected by disturbing those nuclei in different energy states with a radio frequency (RF) electromagnetic pulse. When the system returns to equilibrium, it produces a detectable NMR signal. The application of magnetic field gradients allows the localization of the signal source. The contrast in the image is determined mainly by the amount and mobility of water molecules in the tissue (Grohn and Pitkanen 2007). Relaxation times (T2, transverse; T1, longitudinal) are influenced by the dynamics of water and reflect how hydrogen nuclei return toward equilibrium after excitation by a RF pulse. Modifications of the pulse sequence (excitation and acquisition parameters) allow the modulation of the contrast based on the relaxation and diffusion of water, magnetic coupling between free and bound water, etc. (Grohn anf Pitkanen 2007).

In previous animal MRI studies of CLE, initial increase in T2 signal within a few days after chemical induction of SE was measured in early studies and indicative of edema, cell swelling and increased extracellular water as a result of the injury (Bouilleret, et al. 2000, King, et al. 1991b, Zhong, et al. 1993). This signal increase was followed by normalization after a few days and secondary increase during epileptogenesis (Roch, et al. 2002a). However, other models show a T2 decrease a few hours after SE induction (Bhagat, et al. 2001, van Eijsden, et al. 2004).

Diffusion-weighted imaging (DWI) utilizes the measurement of Brownian motion of water molecules to generate contrast with varying diffusion rates. A decrease in apparent diffusion coefficient (ADC) has been seen in the hippocampus, piriform cortex and amygdala and indicative of early cell loss and ongoing neuronal death only minutes after onset of seizures during SE (Engelhorn, et al. 2007). This initial decrease normalizes after a few days (Wall, et al. 2000, Wang, et al. 1996, Zhong, et al. 1995), at different times for the various brain regions.

Recent volumetric studies in chemically induced SE reported a decrease in hippocampal volume and increased ventricle volume 10 days into epileptogenesis (Wolf, et al. 2002), up to two months after SE (Niessen, et al. 2005), consistent with neuronal loss, hippocampal sclerosis and atrophy. Other long- term studies show decreased temporal lobe volume and progressive decrease in the piriform cortex and amygdala thickness from 9 days up to 6 months after SE induction (Nairismagi, et al. 2004).

Initial changes in T2 affecting the limbic structures usually normalize by day 10 after SE and reappear at day 20 (Dube, et al. 2004, Nairismagi, Grohn, Kettunen, Nissinen, Kauppinen and Pitkanen 2004, Roch, Leroy, Nehlig and Namer 2002a). Care must be exerted when interpreting these relaxation time changes, as T2 increase has been associated with the presence or absence of neurodegeneration (Dube, Yu, Nalcioglu and Baram 2004, Jupp, et al. 2006, Nairismagi, Grohn, Kettunen, Nissinen, Kauppinen and Pitkanen 2004). With the importance and many uses of *in vivo* MRI, continued research is needed to enhance this technique and expand its uses to provide a better understanding of the temporal profile of the pathological changes accompanying epileptogenesis.

Ex vivo **Magnetic Resonance Imaging**

Three-dimensional magnetic resonance microscopy (MRM) can also be used to study animal models of epilepsy. This technique allows for *ex vivo* measurements where motion artifacts are eliminated (Lemaire, et al. 1990). This allows the signal-to-noise ratio to be optimized. Moreover, prolonged scan times and higher field strengths are not limiting factors as with *in vivo* measurements (Guilfoyle, et al. 2003). This *ex vivo* MRI technique allows greater sensitivity in visualizing pathological changes in the brain. Previous studies have shown a strong correlation between T2-weighted signal changes in high-resolution MRI of paraformaldehyde-fixed rat brains and the histological damage in the kainate-induced model of SE (Tiina-Riikka, et

al. 2001). These studies have also shown that MRI *ex vivo* is sensitive enough to detect layer-specific damage in the rat brain after SE, which is not possible with *in vivo* imaging.

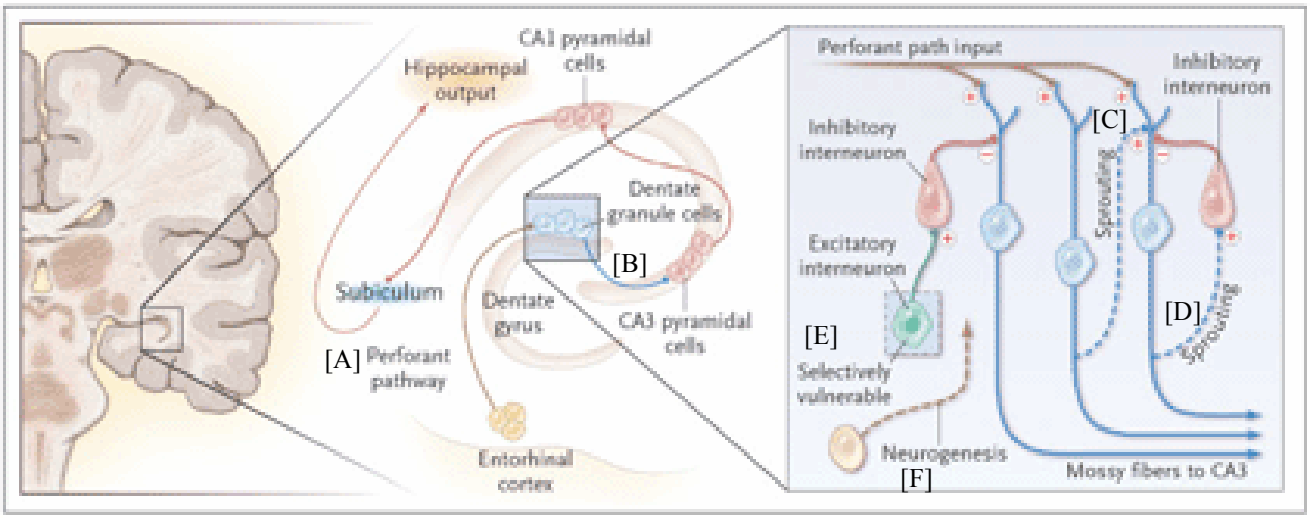

Figure 1-1. Hippocampal Sclerosis. Hippocampal sclerosis is the most common identified pathological feature in cases of mesial temporal-lobe epilepsy. Normally, input to the hippocampus comes from the entorhinal cortex to the dentate granule cells through the perforant path [A]. Dentate granule cells project to the CA3 sector as the first step in the hippocampal output pathway [B]. A close-up of the dentate granule-cell layer reveals several morphologic changes characteristic of hippocampal sclerosis that may play a part in epileptogenesis. Newly sprouted mossy fibers from dentate granule cells can synapse on dendrites of neighboring dentate granule cells, resulting in a recurrent excitatory circuit [C]. They can also sprout onto inhibitory interneurons [D]. Excitation interneurons, which normally activate inhibitory interneurons, may be selectively vulnerable to brain insults [E]. Finally, neurogenesis of new dentate granule cells continues into adult life, and these neurons may integrate themselves into abnormal circuits [F] (from Chang and Lowenstein 2003).

CHAPTER 2
MATERIALS AND METHODS

Animal Preparation

The present study was carried out in accordance with National Institutes of Health guidelines for the care and use of animals and approved by the Institute of Animal Care and Use Committee (IACUC) of the University of Florida. Sprague Dawley (Harlan, Indianapolis, IN) male 50-day-old rats, weighing 304 g ± 77 g, were used in the experiments. Three groups of animals were studied. One group of experimental animals received chronic microwire electrodes to stimulate the hippocampus and induce SE. An implanted control group consisted of animals that were subjected to the same anesthesia, surgical time and electrode implantation as the first group of injured animals but were not stimulated into status epilepticus. A third group consisted of animals which were not implanted with electrodes and served as naïve controls.

Implantation of Hippocampal Electrodes

Animals were pre-medicated with a 2 mg subcutaneous injection of Xylazine (Phoenix Pharmaceutical, St. Joseph, MO), anesthetized with 1.0 – 2.0 % Isoflurane (MINRAD, Bethlehem, PA) and positioned in a Kopf (David Kopf Instruments, Tujunga, CA) stereotactic frame. A midline incision was made in the scalp, and all soft tissue was loosened from the dorsum of the skull. A craniotomy was drilled for electrode placement such that the long axis extended from 1.7 mm lateral to 3.5 mm lateral from bregma and the dura was removed. A pair of 50μm gold-plated tungsten wires (Plastics One, RoanokeVA) were stereotactically implanted in the ventral hippocampus (-5.3 mm posterior, 4.9 mm lateral, right of Bregma, 5 mm ventral) in each rat brain. The electrodes were chronically secured with Methylmethacrylate (Plastics One, RoanokeVA) that was anchored to 4 plastic micro screws driven into the skull (Sanchez, 2006).

Induction of Status Epilepticus, Video Monitoring and Analysis of Spontaneous Seizures

One to two weeks after surgery, the implanted wires were used to attempt the induction of self-sustained status epilepticus (SE, Bertram et al., 1993). A suprathreshold stimulus of 334 ± 159 μA was delivered to the implanted electrodes for 88 ± 26 minutes using 10 s pulse trains of 20 ms period, with 1 ms duration, biphasic square waves with a 2 s delay between pulse trains. The behavior of the animals was video monitored starting 15 days after stimulation and over a period of eight weeks. Seizure detection was performed visually using behavioral (video) monitoring by a veterinarian and behavioral neuroscientist. A behavioral seizure score (BSS) out of 5 was determined for the SE animals in this study using the standard Racine scale (0, no change; 1, wet dog shakes; 2, head bobbing; 3, forelimb clonus; 4, forelimb clonus and animal rearing; 5, rearing and falling). Seizure activity was assessed using the standard Racine scale; only grades 3 through 5 seizures could be determined from video recordings alone.

***In vivo* MR Imaging**

Animals were imaged before and after electrode implantation to serve as their own controls and 3, 5, 7, 10, 20, 40, 60 days after SE to monitor temporal changes (Figure 2-1). Animals were initially anesthetized with 4 % isoflurane in O_2 at 2.0 L/min and injected subcutaneously with 0.8 mg of Xylazine and 2 mL of lactated Ringers solution (Hospira, Lake Forrest, IL) before imaging in the magnet to maintain the physical condition of the rats during the extended MRI scan sessions.

Each animal was placed in a supine position, in a custom- made MRI compatible stereotaxic frame and cradle, to allow repeatable positioning and prevent motion artifacts. A custom-built linear surface coil was used to measure the MR images. A 130 degree arc, 3.5 cm rectangular linear coil was constructed on a 4.0 cm diameter half cylinder to fit animals with

implanted electrodes. This coil features distributed capacitance, balanced impedance matching and a cable trap.

Anesthesia for each rat in the magnet was maintained through a nose cone with a mixture of 1.0 – 2.0 % isoflurane with oxygen at a flow rate of 1 L/min. Respiration was monitored during data acquisition and kept between 30 and 50 breaths/ min by modulating the concentration of isoflurane. Core body temperature was also monitored during experiments by using a rectal probe and kept between 36^{o}C and 37^{o}C; physiological temperature was maintained using heater air flow (SA Instruments, Stony Brook, NY).

In vivo High Resolution MR Imaging Data Acquisition

All in vivo MRI measurements were performed on an 11.1 T, 40 cm horizontal bore magnet at 470 MHz (Magnex Scientific, Abingdon, UK) by using a Bruker Avance console (Bruker NMR Instruments, Inc., Billerica, MA) and 200 mT/m actively shielded gradients. All data acquisition was performed with Bruker ParaVision software. To adjust the position of the image field of view, three-axis pilot images were collected with a T1-weighted coronal spin echo scan using a RARE factor of 4, TR = 1500 ms, TE = 7 ms, a field of view (FOV) of 30 x 30 x 15 mm, matrix size of 128 x 128 with 15, 1 mm thick slices, spectral width of 90 kHz and 4 averages. To visualize the pathology in the brain, a T2-weighted coronal multiple-slice spin echo image data set was acquired over 15 slices of 1 mm thickness and no gap between slices, with a TR = 3000 ms, TE = 12.5 ms, 8 averages, RARE encoding factor of 8, spectral width of 40 kHz, FOV of 30 x 30 x 15 mm and a matrix of 256 x 256.

To quantify T1 relaxation times, multiple-slice spin echo coronal T1-weighted images were acquired over 9 slices of 1 mm thickness with 1.5 mm distance between slice centers, with TR = 4000, 2000, 1000, 500, 250 ms, TE = 15 ms, 2 averages, spectral width of 20 kHz, a FOV of 30 x 30 x 13.5 mm and a matrix size of 100 x 100. To quantify T2 relaxation times, a series of T2-

weighted spin echo coronal scans were acquired over 9 slices of 1 mm thickness with 1.5 mm distance between slice centers, with TR = 2000 ms, TE = 15, 30, 45, 60, 75 ms, 2 averages, spectral width of 70 kHz, a FOV of 30 x 30 x 13.5 mm and a matrix of 100 x 100. The total acquisition time was 25.83 min for T1-weighted images and 33.33 min for T2-weighted scans.

Ex vivo MR Imaging

High-field, high-resolution MR imaging was used to visualized the locations of pathology in the excised fixed animal brains. After finishing the *in vivo* MRI study (8 weeks after SE), the animals were deeply anesthetized, sacrificed and transcardially perfused according to the Timm fixation protocol: 0.37% sulfide solution (30 ml/min) for 10 min followed by 4% paraformaldehyde in 0.1 *M* phosphate buffer, pH 7.4 (30 ml/min), +4°C, for 10 min (Nairismagi et al, 2004). The electrodes were removed, and the intact brains extracted from the skulls and post-fixed in 10% formalin. Prior to *ex vivo* MR imaging, the intact fixed brains were soaked in phosphate buffer solution (PBS) for about 24 hours to wash out residual fixative.

The excised brains were then placed in an 18 mm tube containing fluorinated oil and imaged at 750 MHz in a 17.6 T, 89 mm bore Bruker Avance MR instrument (Bruker NMR Instruments, Billerica, MA). All data acquisition was performed with Bruker ParaVision software. Three-dimensional MR microscopy (MRM) images were acquired with a 3D gradient echo pulse sequence with TR = 150 ms, TE = 15 ms. The image field-of-view was 30 mm × 18 mm × 15 mm in a matrix of 400 × 240 × 200, and the data were acquired in a total data acquisition time of 2 h per signal average. Through experimentation, 2 averages (4 h) provided the optimum compromise between signal-to-noise ratio and measurement time. All the MRM images were acquired with a resolution of 75 × 75 × 75 μm^3. A 3D Fourier transformation was applied to the acquired data matrix to produce the 3D image, which was then interpolated using a

bilinear interpolation, by a factor of 2 in each dimension to produce an image with a display resolution of 37.5μm.

To quantify T1 relaxation times, multiple-slice spin echo coronal T1-weighted images were acquired over 15 slices of 0.5 mm thickness with 0.6 mm distance between slice centers, with TR = 5000, 2000, 1000, 500, 300 ms, TE = 10 ms, 2 averages, spectral width of 38 kHz, a FOV of 19 x 18 mm and a matrix size of 128 x 128. To quantify T2 relaxation times, a series of T2-weighted spin echo coronal scans were acquired over 15 slices of 0.5 mm thickness with 0.6 mm distance between slice centers, with TR = 3000 ms, TE = 15, 30, 45, 60, 75 ms, 2 averages, spectral width of 44 kHz, a FOV of 36 x 18 mm and a matrix of 128 x 128. The total acquisition time was 37 min for T1-weighted images and 1 h for T2-weighted scans. Brains were placed in fixative right after *ex vivo* imaging.

Histological Procedures

Fixation

Following *ex vivo* MR imaging, the excised brains were cryoprotected in 30% sucrose in PBS and sodium azide before they were processed for histology. The brains were then blocked, frozen in dry ice and sectioned in the coronal plane into 50 μm-thick sections on a freezing microtome. Sections were collected in PBS and mounted on gelatin-coated slides. Adjacent series of sections were used for Nissl, Perl, Fluoro-Jade C, Timm and Black Gold staining.

Nissl Staining

Cellular morphology of the different brain areas was assessed using Nissl staining. The slide-mounted brain sections were soaked in Cresyl Violet solution for 10 min, dehydrated through a graded series of ethanol–water solutions, cover-slipped, and analyzed under a bright field microscope.

Perl's Staining

For pathological iron visualization, the brain sections were incubated in Perl's solution (1:1, 5% potassium ferrocyanide and 5% HCl) for 45 minutes, washed in distilled water, and incubated again in 0.5% diamine benzidine tetrahydrochloride for 60 minutes (Hill, 1984). Half of the slides were then counter-stained with Cresyl Violet.

Fluoro-Jade C

An adjacent series of sections was stained with Fluoro-Jade C for detection of degenerating neurons. Slides were first immersed in a basic alcohol solution consisting of 1% sodium hydroxide in 80% ethanol for 5 min. They were then rinsed for 2 min in 70% ethanol, for 2 min in distilled water, and then incubated in 0.06% potassium permanganate solution for 10 min. Following a 1-2 min water rinse, the slides were then transferred for 10 min to a 0.0001% solution of Fluoro-Jade C dissolved in 0.1% acetic acid vehicle. The proper dilution was accomplished by first making a 0.01% stock solution of the dye in distilled water and then adding 1ml of the stock solution to 99ml of 0.1% acetic acid vehicle. The working solution was used within 2 h of preparation. The slides were then rinsed through three changes of distilled water for 1 min per change. Excess water was drained onto a paper towel, and the slides were then air dried for at least 5 min. The air dried slides were then cleared in Xylene for at least 1 min and then cover-slipped with non-fluorescent mounting media.

Timm Staining

Synaptic reorganization through mossy fiber sprouting was analyzed from sections stained with the Timm sulfide silver method (Danscher, 1981). Half of the slides were counter-stained with Cresyl Violet to stain for cytoplasmic RNA-rich ribosomes, as well as the nuclei and nucleoli of the nerve cells.

Black Gold Staining

In order to localize the presence of normal or pathological myelin, the slides were stained with haloaurophosphate complex, called Black Gold. A 0.2% solution of Black Gold was made by adding 100mg of Black Gold to 50 ml of 0.9% NaCl and then heating it to 60 degrees C. The slide mounted tissue sections were transferred to this warm Black Gold impregnating solution in the oven for 12-18 minutes. At this point, the stain was intensified by incubating the sections for 10-15 minutes in a 60 degrees C solution of 0.2% potassium tetrachloroaureate (Alrich Chem., Milwaukee, WI) dissolved in 0.9% saline. The sections were then rinsed for 2 minutes in distilled water, fixed for 3 minutes in a sodium thiosulfate solution, and then rinsed in tap water for at least 15 minutes (three 5 minute changes). Slides were dehydrated through gradated alcohols. The dehydrated sections were cleared in Xylene (Fisher Scientific, Pittsburgh, PA) for at least 2 minutes and then cover-slipped with plastic mounting media (Schmued, 1999).

Data Analysis

I*n vivo* and *ex vivo* general MR image processing and analysis was performed by using custom software written in the Interactive Data Language software (IDL, from Research Systems, Boulder, CO). Using a rat brain anatomical reference atlas (Paxinos, 1997), regions of interest (ROIs) were chosen around the following structures in both the right and left brain hemispheres: hippocampus and two hippocampal subregions (CA1 and dentate gyrus regions), fimbriae/ lateral ventricles, entorhinal cortex, piriform cortex, amygdala, dorsal thalamus and retrosplenial cortex (Figure 2-2). All slices containing these ROIs were chosen for quantitative T1 and T2 relaxation measurements using in house MRI Analysis Software (MAS) written in IDL.

For SE animals, *in vivo* measurements were averaged within three time periods: before stimulation into SE, between 3 and 10 days after SE (latent period) and 20 to 60 days after SE

(beginning of spontaneous seizures). *In vivo* T1 and T2 measurements for each ROI were assessed for statistically significant differences between time periods using paired Student's *t* tests (R, Boston, MA). A p value < 0.05 was considered to be significant. For *ex vivo* measurements, statistically significant differences between the SE and control groups were assessed using unpaired Student's *t* test between the two groups.

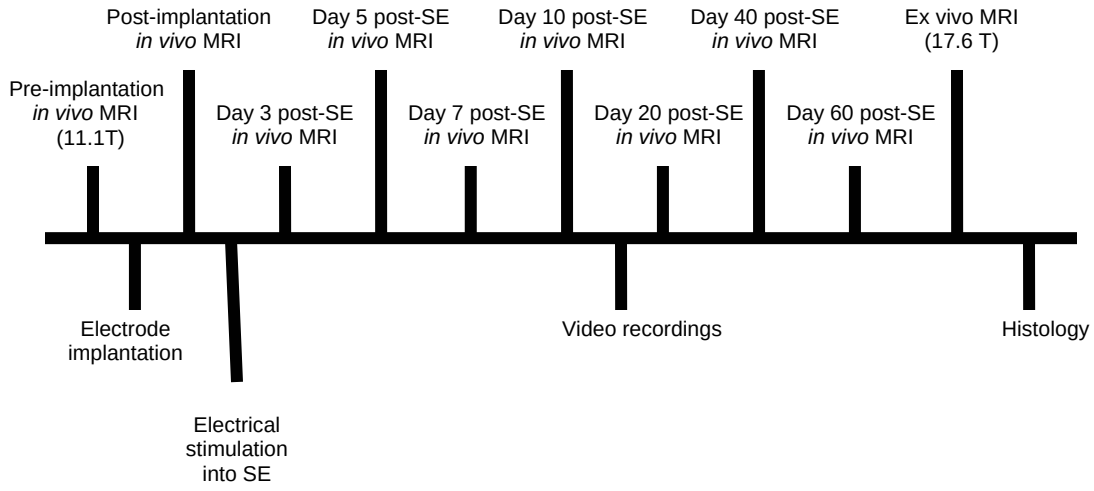

Figure 2-1. Stimulation and MR imaging timeline.

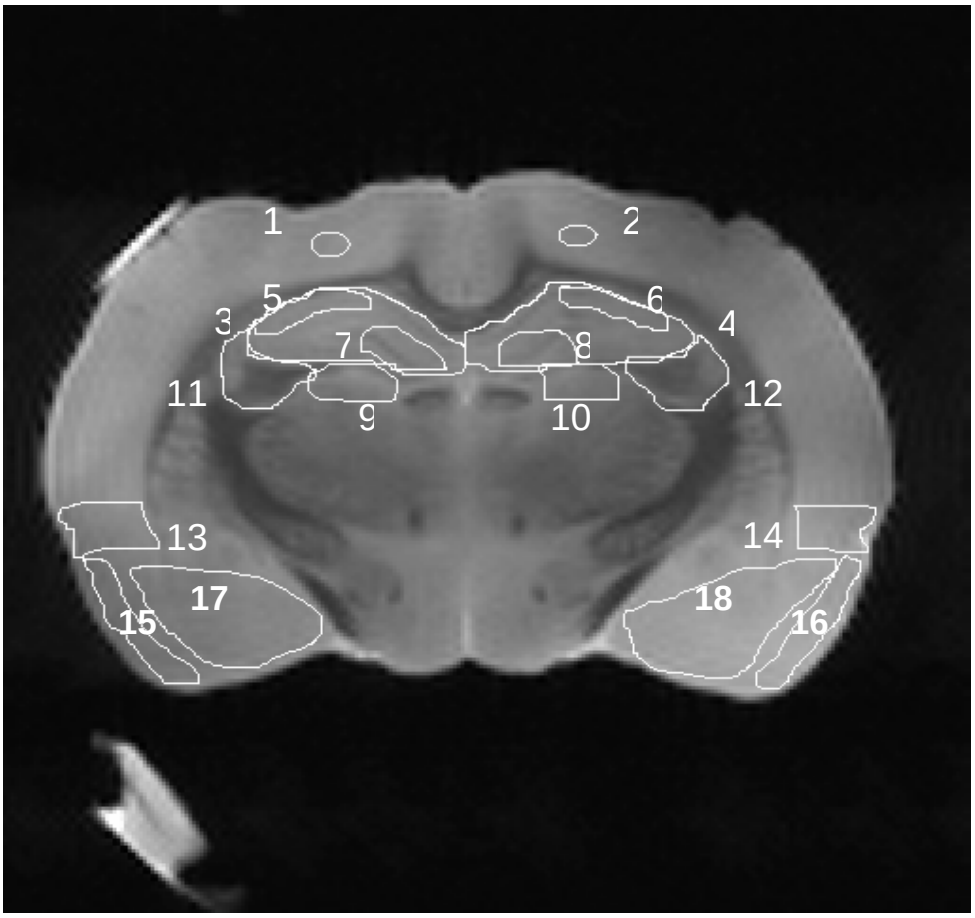

Figure 2-2. Coronal T2-weighted image of implanted control excised brain showing anatomical regions of interest: 1, 2- retrosplenial cortex; 3, 4 -hippocampus; 5, 6 - CA1; 7, 8 – dentate gyrus; 9, 10 - dorsal thalamus; 11, 12 – lateral ventricles/ fimbriae; 13, 14- entorhinal cortex; 15, 16- piriform cortex; 17, 18- amygdala.

CHAPTER 3
RESULTS

Animal Behavior

Control animals that were not implanted with electrodes or implanted but not stimulated did not exhibit any behavioral alteration. Thus electrode implantation alone did not induce epileptogenesis. Of the animals that were stimulated in the study, one did not undergo SE and was found to have electrodes implanted in the medial geniculate nuclei instead of the hippocampus, as verified with MRI after electrode implantation. One of the animals that reached SE died 12 days after stimulation from unknown causes. Another animal that attained SE was sacrificed at 9 days because of health complications and was kept for histological analysis. The animals that attained SE immediately following the onset of stimulation demonstrated "wet dog shakes" and seized several times during the procedure. After the stimulus was ended, hyperactivity and seizing was observed for approximately 8 hours afterwards.

One animal started seizing for the first time 12 days after stimulation. Video analysis of seizures indicated that 4 rats had spontaneous seizures at 20 days after SE, and one had seizures beginning at 29 days after SE. At 20 days after SE in spontaneously seizing rats, the number of daily spontaneous seizures varied between 1 and 3 (mean, 2 ± 1; $n = 3$) and at 29 days between 0.7 and 1.4 (mean, 1 ± 0.2; $n = 5$). The spontaneously seizing animals had an average of less than 1 seizure per day and continued seizing until the end of the video recording period (60 days after stimulation). However, one animal seized with high frequency (greater than 2 seizures per day) for the first 2 weeks, but no seizures were observed 31 days after SE. The mean score indicating the behavioral severity of spontaneous seizures was 3.2 ± 0.5 at 20 days and 3.3 ± 0.7 at 60 days. Only seizures grades 3 to 5 could be observed by the veterinarian and were reported.

In vivo High Resolution MR Imaging

All relaxation time data from pre-implantation MRI scans were compared to determine biological variability between animals, and relaxation times in the same region of the frontal cortex, away from the site of electrode implantation, were measured over time to confirm repeatability of the measurements for each animal. The relaxation time variability between animals pre-implantation was low; average standard deviation was 4.5 ± 2.1 % between all animals for all regions of interest. No significant changes were observed in naïve control and implanted control animals (Figure 3-1) and non-seizing injured animals over the 60 days of imaging (standard deviation 2.9 ± 0.8 %). Control animals did not show any significant difference in their T1 and T2 values between right and left hemispheres ($p < 0.05$, using paired t-test). T1 measurements followed the same pattern of variation as the T2 measurements for the various regions of interest, except that T1 changes were less significant than T2 changes (Figure 3-2). The average T1 relaxation times measured from control animals were 3.1 ± 0.05 s (piriform cortex), 3.0 ± 0.01 s (amygdala), 2.7 ± 0.9 s (thalamus), and 2.9 ± 0.01 s (hippocampus).

Figure 3-3 shows T2-weighted MRI scans acquired over the course of *in vivo* imaging for an epileptic animal. Quantitative MRI relaxation time measurements were performed *in vivo*, in control and stimulated animals at 3, 7, 10, 20, 40 and 60 days after stimulation. These T2 measurements were averaged over the pre-stimulation period, the latent period (3 to 10 days after SE) and the spontaneous seizure period (20 to 60 days after SE) for ipsilateral and contralateral regions of interest (Figure 3-4). The average T2 relaxation times measured from control animals were 38.7 ± 2.1 ms (piriform cortex), 38.2 ± 1.7 ms (amygdala), 34.2 ± 1.4 ms (thalamus), and 37.6 ± 1.2 ms (hippocampus). The rat that survived SE but did not develop epilepsy presented no modification of the signal on T2-weighted images over the entire course of *in vivo* imaging, and the T2 relaxation times remained in the range of values for control animals at all time points. In

epileptic animals, the retrosplenial cortex showed a significant T2 decrease on the ipisilateral side to stimulation 3 to 10 days after stimulation ($p < 0.05$) compared with control values (Figure 3-4). The hippocampus and the CA1 subregion also showed significant T2 decrease bilaterally ($p < 0.05$) during the latent period. On the other hand, the lateral ventricle/ fimbriae areas, piriformic cortices and the amygdala showed a statistically significant T2 increase bilaterally 3 to 10 days after stimulation ($p < 0.05$), which peaked at 3 days after SE and returned to baseline before 10 days (Figure 3-5). This T2 increase in the lateral ventricle/ fimbriae areas correlated with a bilateral increase in ventricular volume observed and quantified over time on T2-weighted images using the Slicer software (Figure 3-6).

The ventricle/fimbriae areas showed further significant T2 increase 20 to 60 days after stimulation bilaterally, while the amygdala on the contralateral side to stimulation and piriformic cortex on both sides showed a significant decrease in T2 values after 20 days compared to 3 to 10 days after SE ($p < 0.05$). The retrosplenial cortex, hippocampus (including dentate gyrus and CA1 subregions), entorhinal cortex and dorsal thalamus showed a significant T2 decrease bilaterally 20 to 60 days after stimulation compared to control values ($p < 0.05$) (Figure 3-4). The epileptic animals showed interindividual differences in T2 variations at each time point and in their seizing patterns, possibly due to the slight differences in location of the stimulating electrodes implanted in the ventral hippocampus.

Ex vivo MR Microscopy

Ex vivo MR images had greater resolution and more defined areas of pathology (i.e. neuronal loss, cavitation, iron deposition) in the epileptic brains compared with *in vivo* images (Figures 3-7,8). Areas of hypointensities were visible in the CA1 subregions of the hippocampus and dorsal thalamus bilaterally, as well as the piriform cortex. Atrophy of the hippocampus and enlargement of the ventricles bilaterally were also evident. Quantification of T_2 measurements

for *ex vivo* data (Figure 3-9) supported the qualitative observation of the MR images. T2 values were decreased in the hippocampus bilaterally, especially in the CA1 subfield, in animals that underwent seizures when compared with control animals ($p < 0.05$, *t* test). Average T2 was also significantly decreased in the piriform cortex and dorsal thalamus bilaterally. On the other hand, T2 was significantly increased in the amygdala on the contralateral side to stimulation. T2 values were dramatically increased in the lateral ventricle/ fimbriae areas bilaterally ($p < 0.05$). No significant differences in T2 measurements were observed between seizing and control animals in the cortex.

Histologic Findings

Data obtained from histological staining helped elucidate pathological changes observed and quantified with *in vivo* and *ex vivo* MR imaging. Electrode tracts were visible on histological sections of implanted animals. Nissl staining showed decreased neuronal density in the hippocampus, particularly in the dentate hilus, and the CA1 and CA3 pyramidal cell layers (Figure 3-10) in epileptic animals sacrificed after 60 days post-SE. Decreased neuronal density was also observed in the amygdala, piriform cortex and the dorsal thalamic nuclei.

Timm staining showed increased density of mossy fiber sprouting bilaterally in the inner molecular layer of the stratum granulosum in epileptic animals (Figure 3-11). Abnormal presence of astroglial cells and degenerating neurons was observed in the CA1 subregion of the hippocampus after Fluoro-Jade C staining in one of the epileptic animals (Figure 3-12) sacrificed after 60 days post-SE. Strong iron deposition was observed in the dorsal thalamic nuclei bilaterally (Figure 3-13) as well as at the site of electrode implantation. Iron deposition was also observed in the inner molecular layer of the stratum granulosum of the dentate gyrus (Figure 3-14). Perl sections counter-stained with Cresyl Violet revealed cavities in the piriform cortex bilaterally with iron deposition and aggregation of microglia around the cavities (Figure 3-15).

Decreased myelin staining in the amygdala, the piriform cortex and the CA1 subfield of the hippocampus were observed after Black Gold staining (Figure 3-16). Enlargement of the ventricles was also visible bilaterally, more pronounced on the contralateral side to stimulation, as well as extensive loss of tissue and decreased thickness in the amygdala and piriform cortex regions.

In one rat sacrificed at day 9 after SE, Perl staining counter-stained with Cresyl Violet showed diffuse iron deposition in the dentate gyrus, as well as cavitation in the piriform cortex with microglia aggregation (Figure 3-17). Fluoro-Jade C staining revealed ongoing degenerating neurons throughout the CA1, CA2 and CA3 pyramidal cell layers of the hippocampus, the dorsal thalamic nuclei and the dentate hili bilaterally (Figure 3-18).

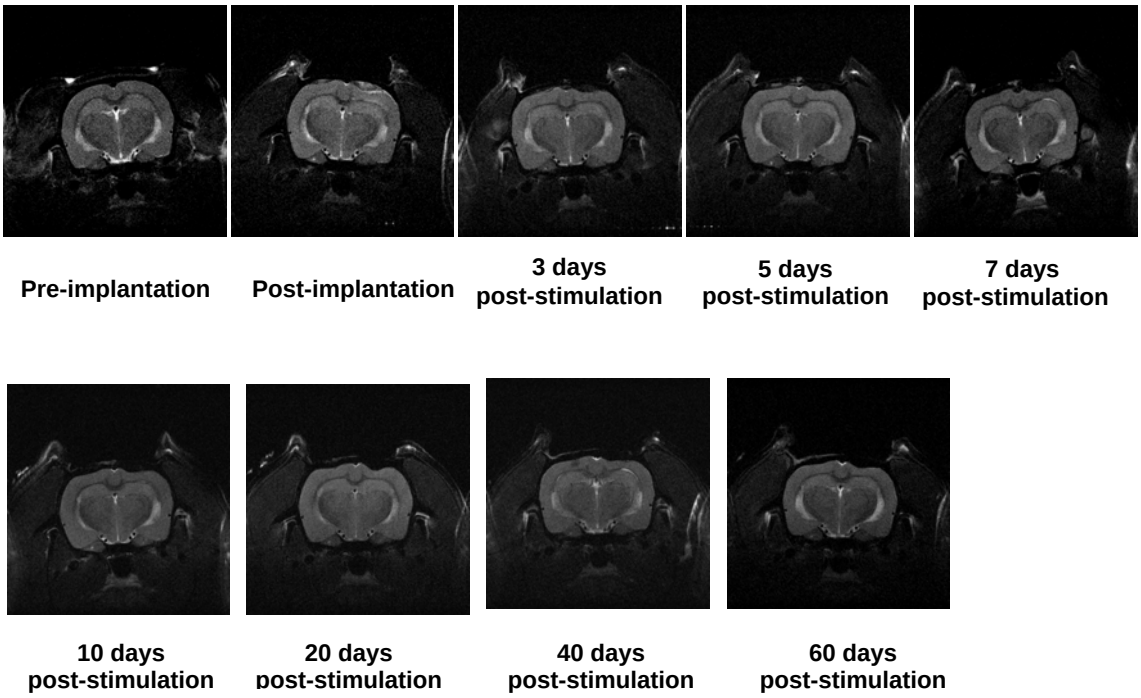

A

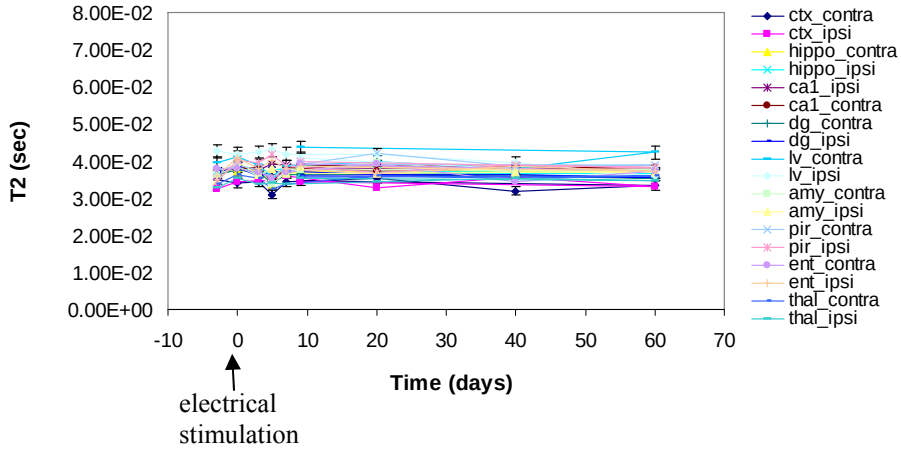

B

Figure 3-1. T2 MR imaging in implanted control. (A) Coronal *in vivo* T2-weighted (TR/TE = 3000/12.5 ms; NA = 8) MRI scans before and after implantation of electrodes and at 3, 7, 10, 20, 40 and 60 days in implanted control animal (MR Rat 9), (B) T2 relaxation measurements versus time after stimulation for implanted control animals. No significant differences were observed in T2 values over time after implantation compared with control values for regions of interest. T0 = electrical stimulation. Error bars represent one standard deviation. Regions of interest: retrosplenial cortex (ctx), hippocampus (hippo), ca1, dentate gyrus (dg), lateral ventricles (lv), amygdale (amy), piriform cortex (pir), entorhinal cortex (ent), thalamus (thal).

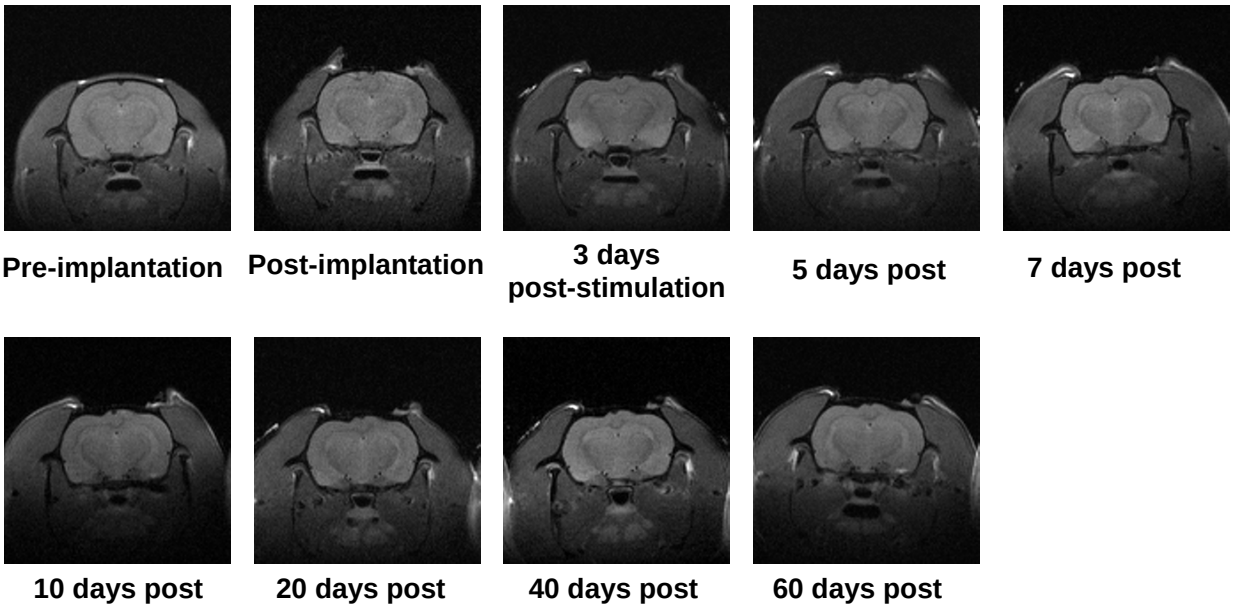

Figure 3-2. Coronal *in vivo* T1-weighted (TR/TE = 1500/7 ms; NA = 4) MRI scans before and after implantation of electrodes and at 3, 7, 10, 20, 40 and 60 days after stimulation in epileptic animal (MR Rat 4).

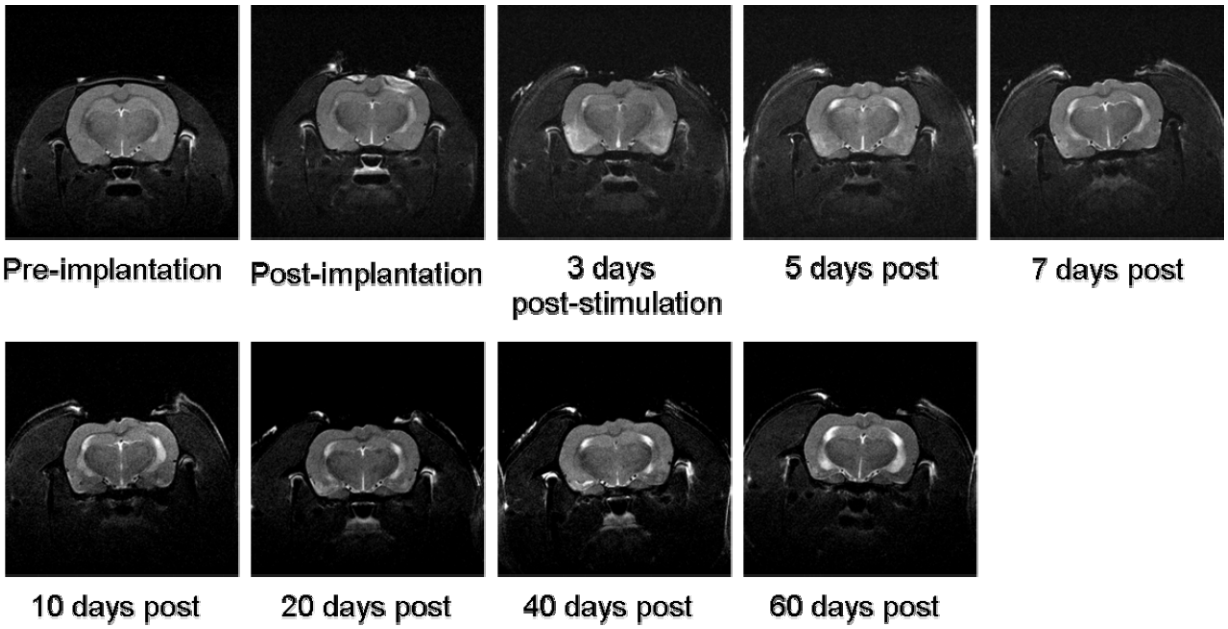

Figure 3-3. Coronal *in vivo* T2-weighted (TR/TE = 3000/12.5 ms; NA = 8) MRI scans before and after implantation of electrodes and at 3, 7, 10, 20, 40 and 60 days after stimulation in epileptic animal (MR Rat 4).

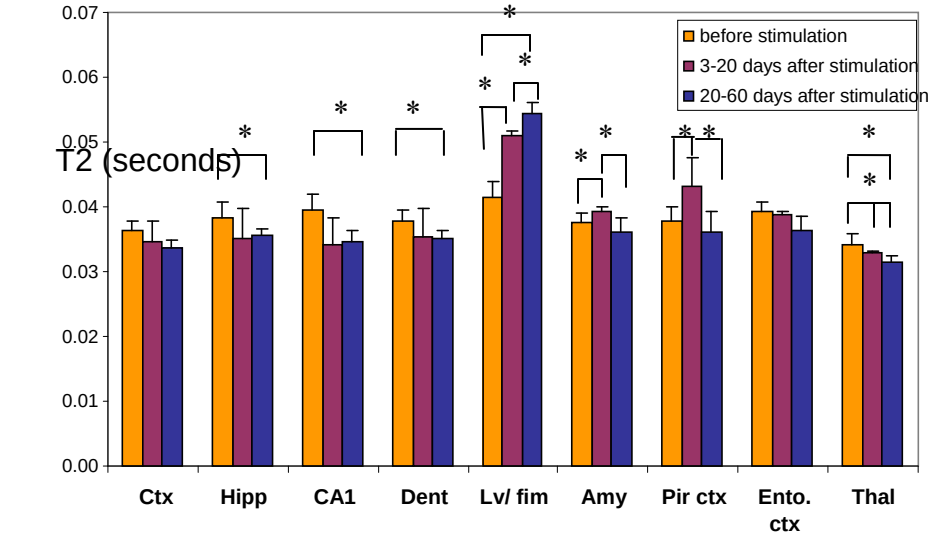

A

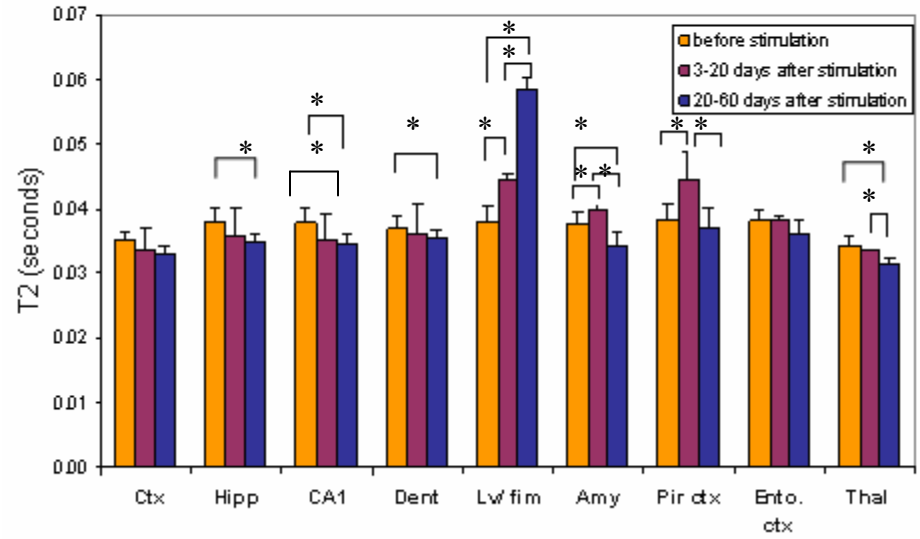

B

Figure 3-4. Average T2 relaxation times in epileptic animals before stimulation 3 to 10 days (latent period) and 20 to 60 days after stimulation (spontaneous seizures), (A) ipsilateral and (B) contralateral to stimulation. Error bars represent one standard deviation. Regions of interest: retrosplenial cortex (Ctx), hippocampus (Hipp), CA1, dentate gyrus (Dent), lateral ventricles/fimbriae regions (LV/fim), amygdala (Amy), piriform cortex (Pir ctx), entorhinal cortex (Ento ctx), thalamus (Thal).

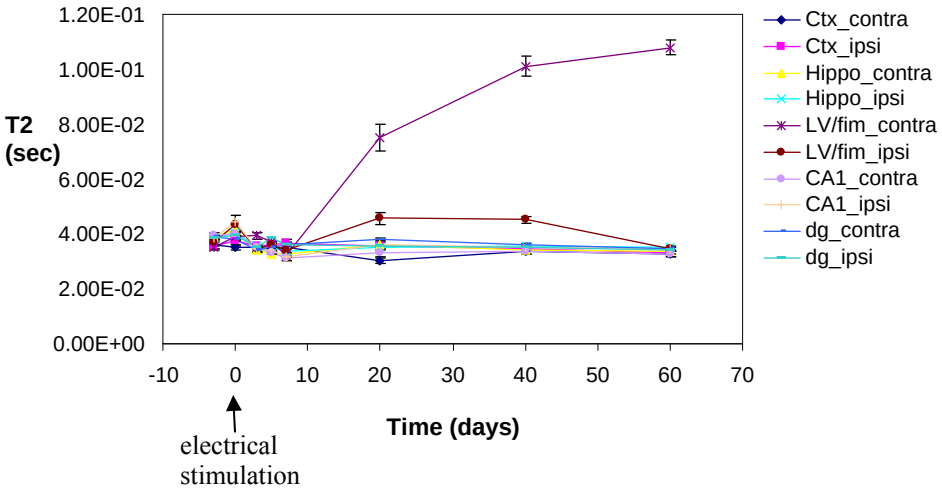

A

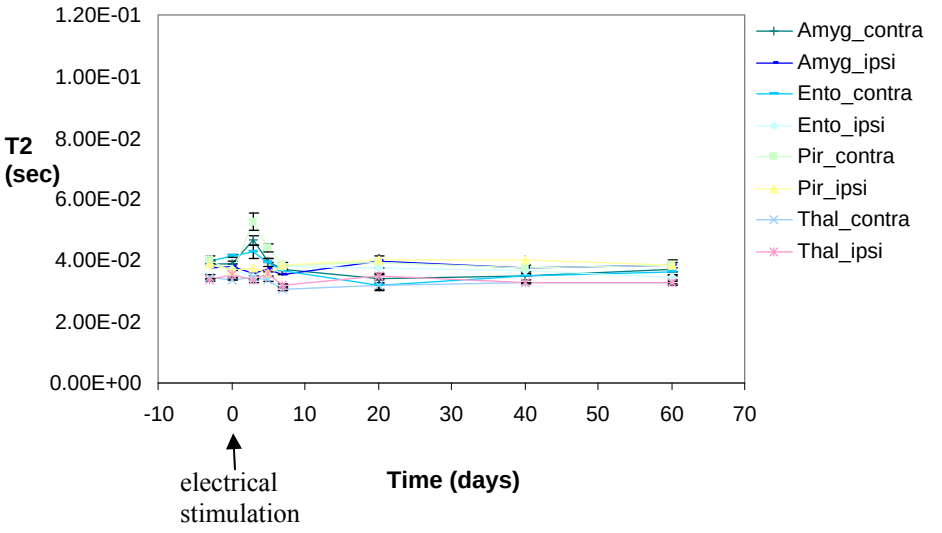

B

Figure 3-5. T2 relaxation times before and after implantation of electrodes and 3, 7, 10, 20, 40 and 60 days after stimulation in epileptic animal (MR Rat 6),in ipsilateral and contralateral ROIs: (A) cortex (Ctx), hippocampus (Hippo), lateral ventricle/ fimbriae (LV/fim), CA1 and dentate gyrus (DG), (B) amygdala (Amyg), entorhinal cortex (Ento), piriform cortex (Pir) and thalamus (Thal). T0 = electrical stimulation. Error bars represent one standard deviation.

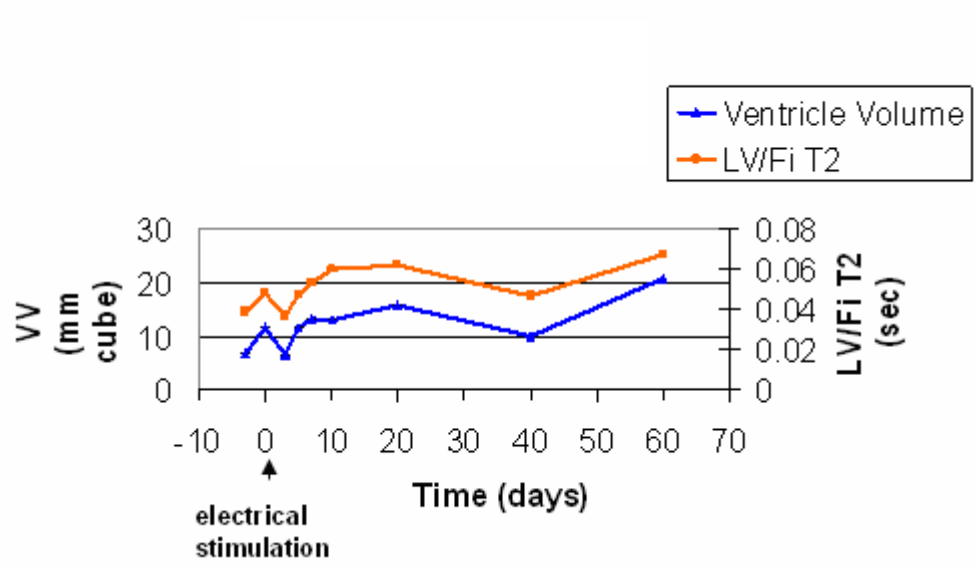

Figure 3-6. Ventricular volume and T2 relaxation times in lateral ventricle regions across time for one epileptic animal (MR Rat 4). LV/Fi = lateral ventricle/ fimbriae region.

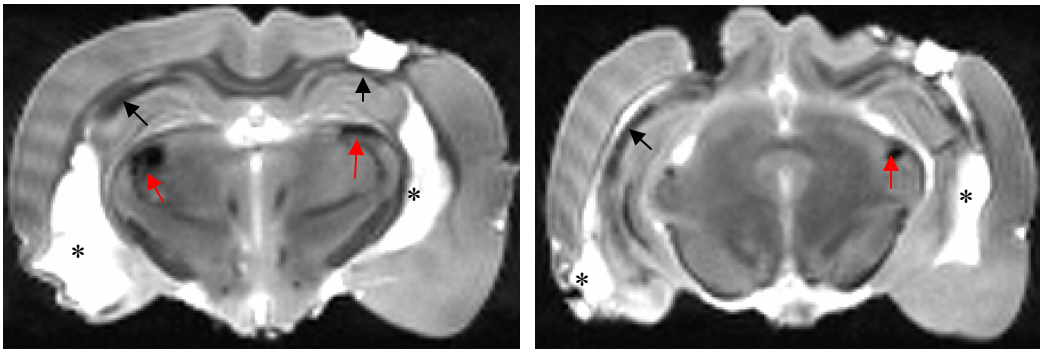

Figure 3-7. Coronal (17.6 T) T2-weighted images of injured excised brain (MR Rat 1), showing hypointense regions in CA1of the hippocampus (black arrows) and the dorsal thalamic nuclei bilaterally (red arrows), hypointense signal in the piriform cortex, increased ventricle areas bilaterally (*) and decreased thickness of piriform cortex and amygdala.

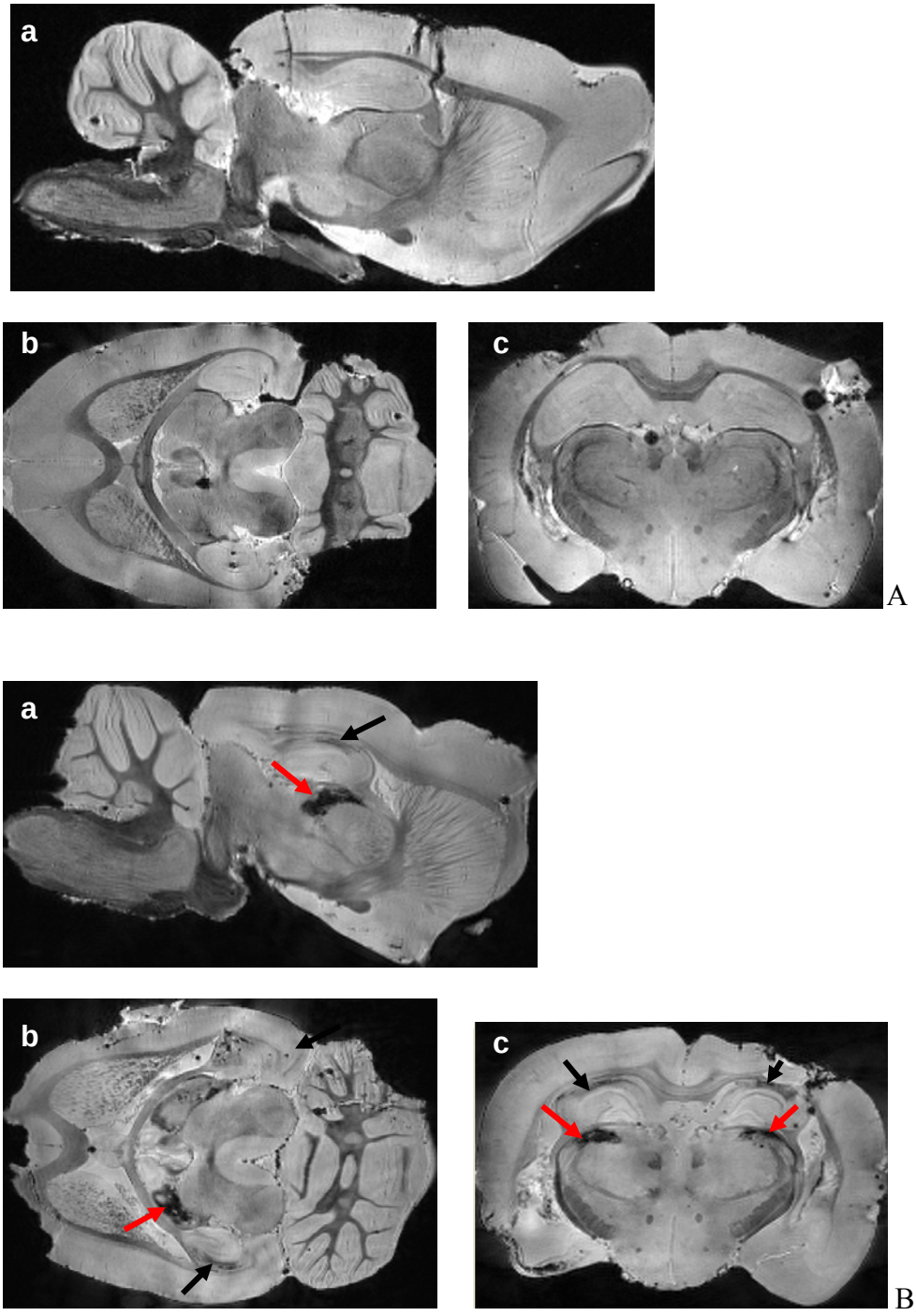

Figure 3-8. (A) 17.6 T sagittal (a), transverse (b) and coronal (c) 3D images of implanted control excised brain (R101). (B) 17.6 T sagittal (a), transverse (b) and coronal (c) 3D images of epileptic excised brain (MR Rat 1). Note the areas of hypointensity within the CA1 subregion of the hippocampus bilaterally (black arrows), as well as the dorsal thalamic nuclei (red arrows) in the epileptic brain.

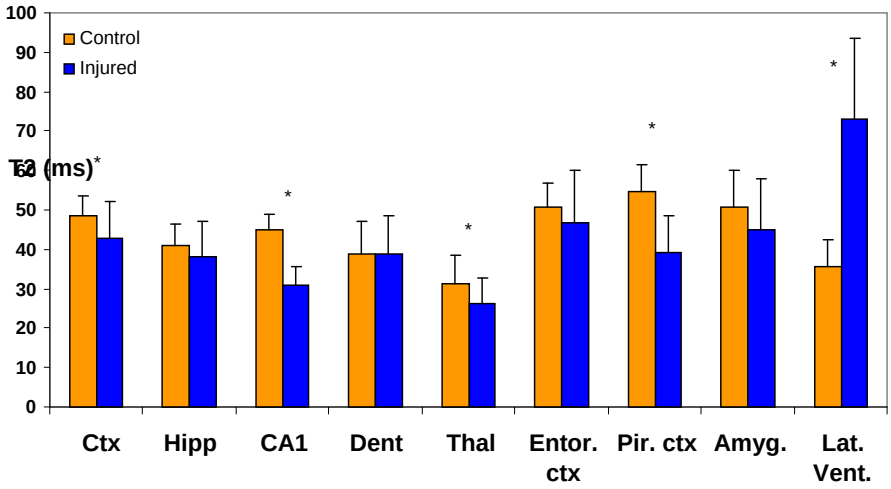

A

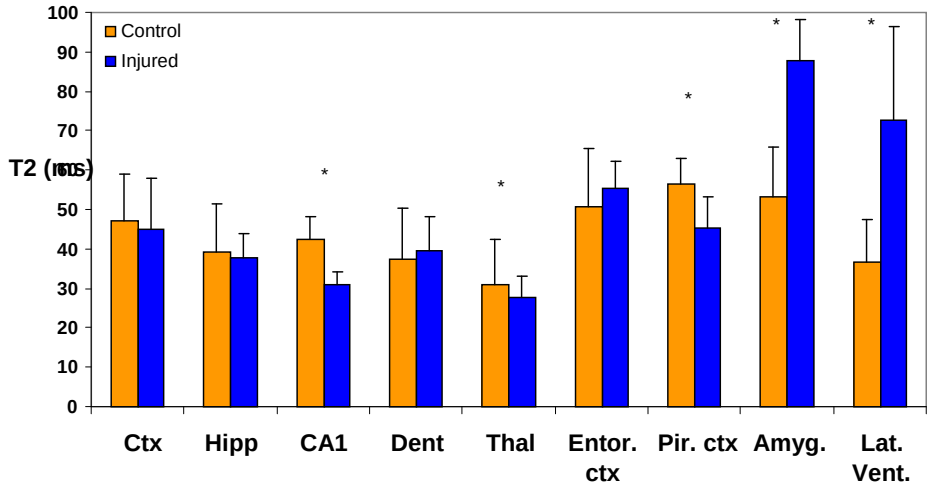

B

Figure 3-9. Average T2 values are presented for various regions for both hemispheres, (A) ipsilateral and (B) contralateral to the side of stimulation. Injury-induced changes are apparent in the contralateral hemisphere and to a lesser degree in the ipsilateral side. The T2 values were found to be significantly different between the control and the injured brains in the CA1 subregion of the hippocampus, as well as the thalamus, amygdala and piriform cortex. (*) $p < 0.05$. Error bars represent one standard deviation.

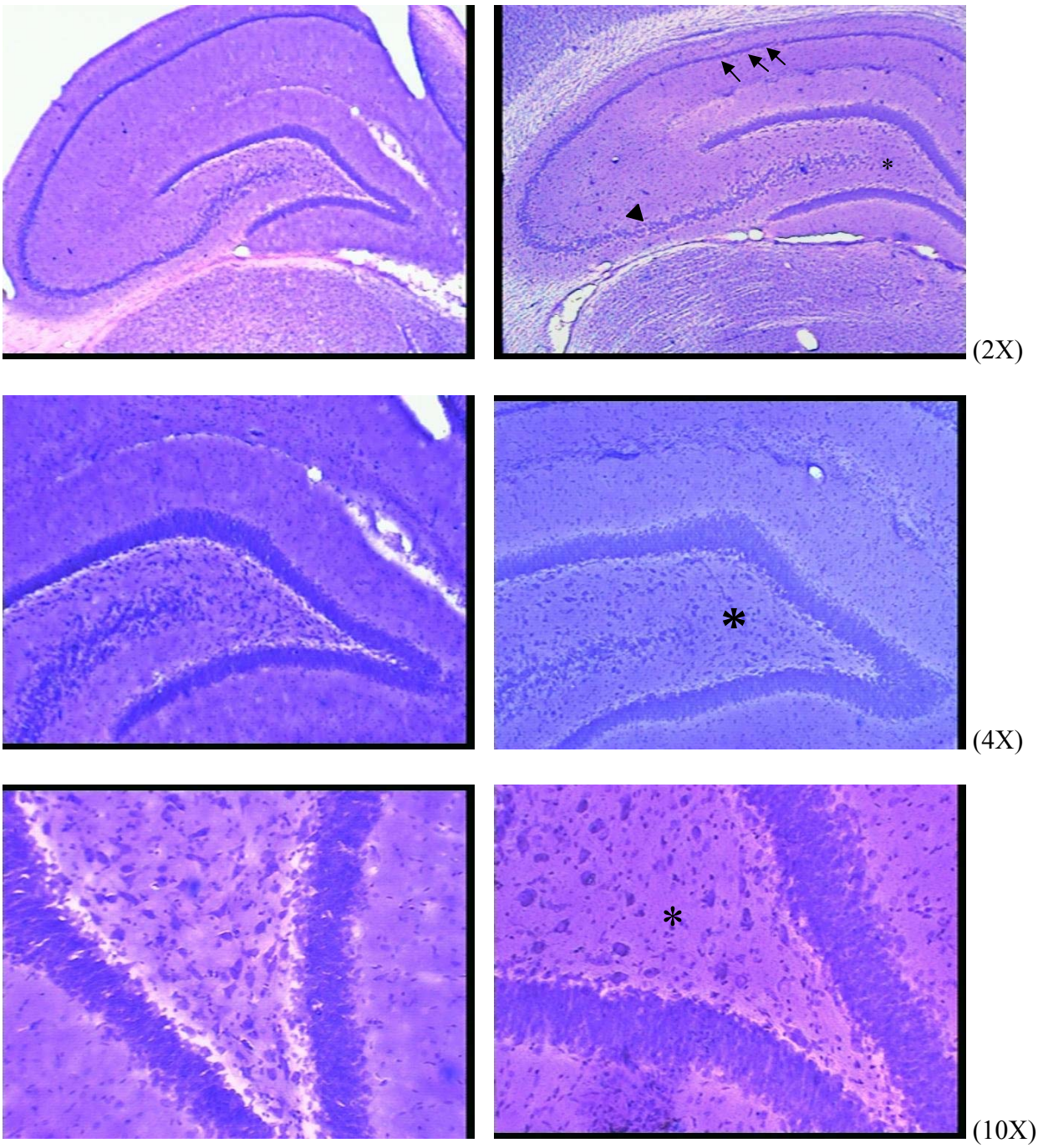

Figure 3-10. Cresyl-Violet staining shows decreased neuronal density in CA3 pyramidal cell layer (arrowhead), CA1 (arrows) and dentate hilus (*) of hippocampus in epileptic animal (MR Rat 5, left) compared to control (MR Rat 9, right).

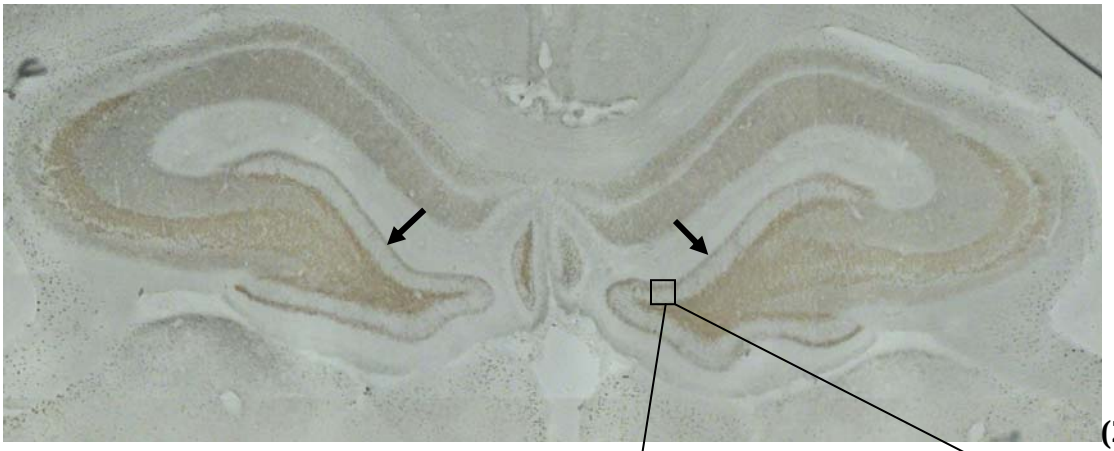

(2X)

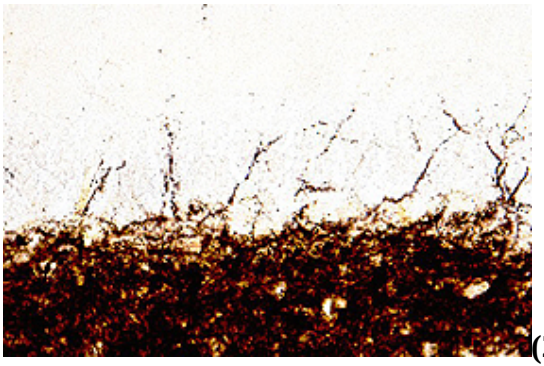

(20X)

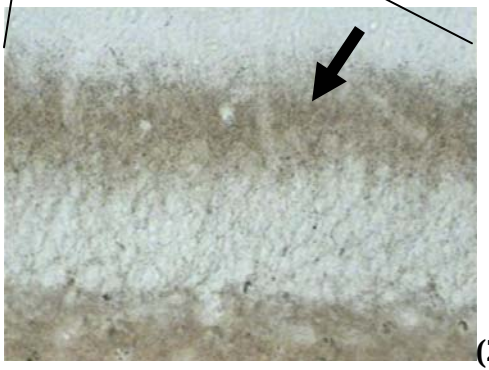

(20X) A

Control

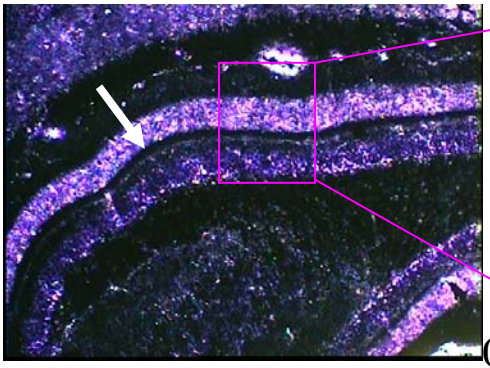

(10X)

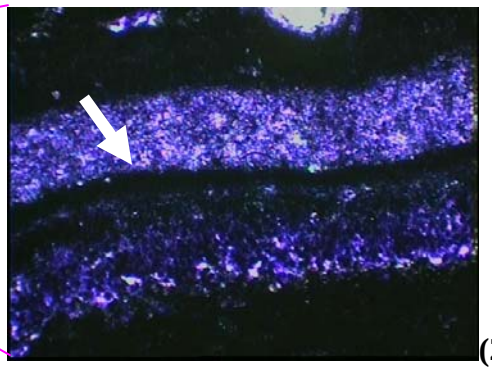

(20X) B

Figure 3-11. (A)Timm staining of epileptic brains 60 days after SE shows mossy fiber terminals in the inner (supragranular) molecular layer of the dentate gyrus bilaterally (arrows). Brown staining shows zinc precipitation along the mossy fibers in the hippocampal formation. This represents aberrant sprouting of the mossy fibers to a region not normally innervated by mossy fibers. High magnification of the granule cell and molecular layers of the dentate gyrus in a control rat brain show little reaction deposits in the molecular layers (from www.fdneurotech.com). (B) Timm sections counter-stained with Cresyl-Violet. White arrows point to mossy fibers stained black.

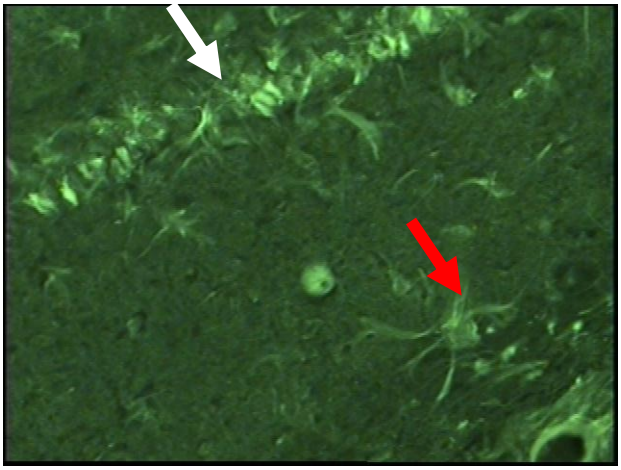

Figure 3-12. Fluoro-Jade C section of one epileptic brain (MR Rat 1) showing the presence of degenerating neurons in the CA1 pyramidal cell layer of the hippocampus (white arrow), as well as the abnormal presence of astroglial cells (red arrow), suggesting possible gliosis in that area.

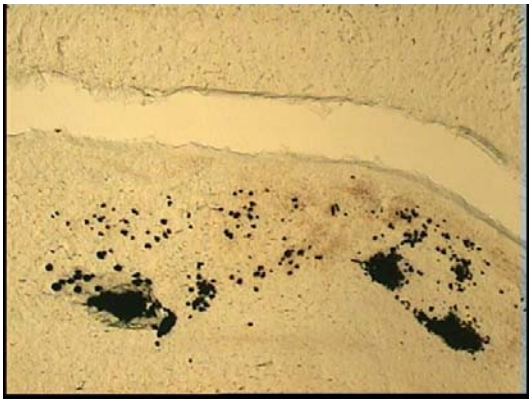

A

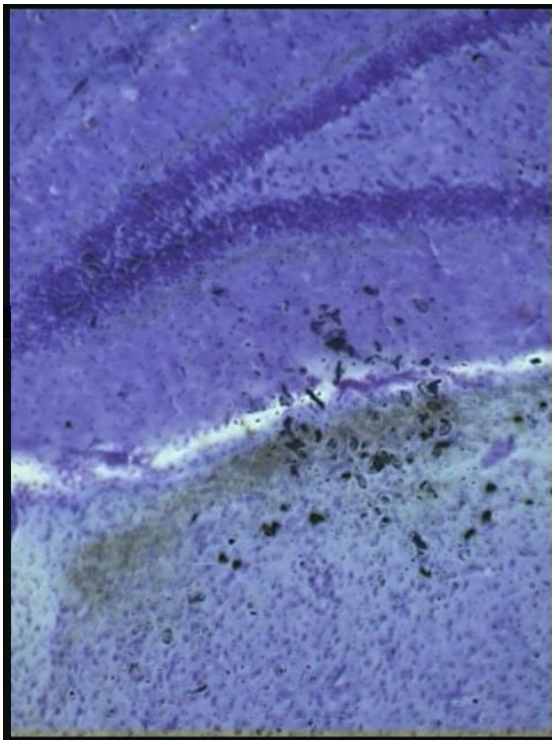

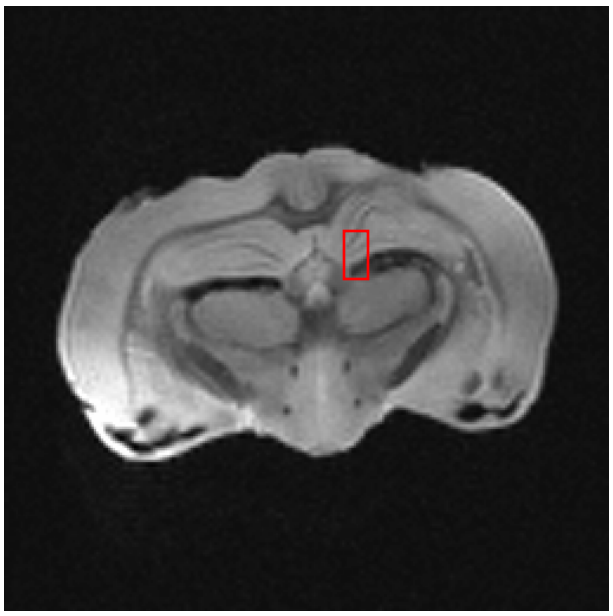

B

Figure 3-13. (A) Perl's staining reveals iron deposition in the dorsal thalamic nuclei bilaterally in epileptic animal (MR Rat 5). (B) Perl section counter-stained with Cresyl- Violet shows iron deposition in the dorsal thalamic nuclei. The corresponding region is enclosed in the rectangle on a T2-weighted *ex vivo* MR image of the same epileptic animal and appears as an area with hypointense signal.

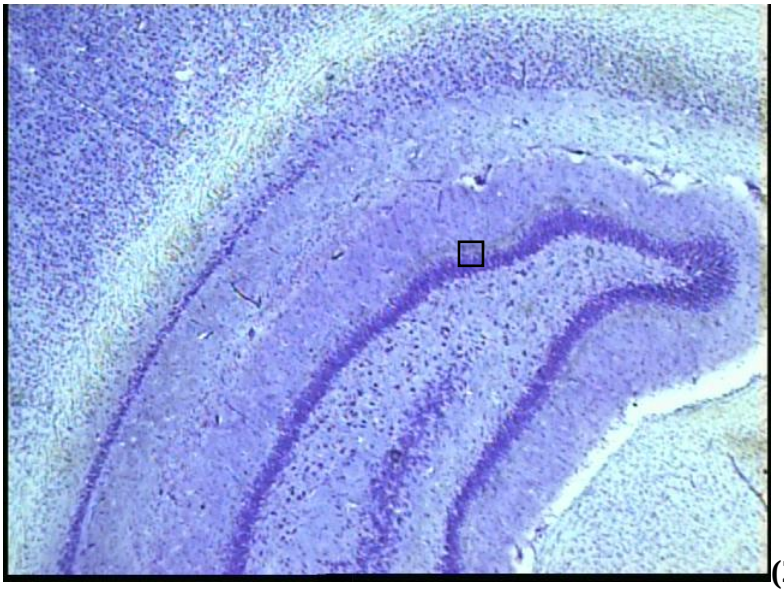

(2X)

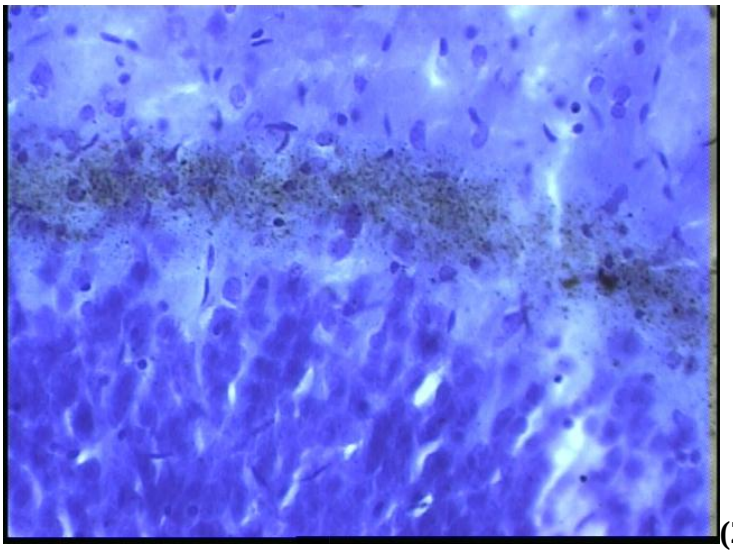

(20X)

Figure 3-14. Perl's reaction counter-stained with Cresyl-Violet shows iron deposition in the inner molecular layer of the stratum granulosum of the dentate gyrus in epileptic brain (MR Rat 4).

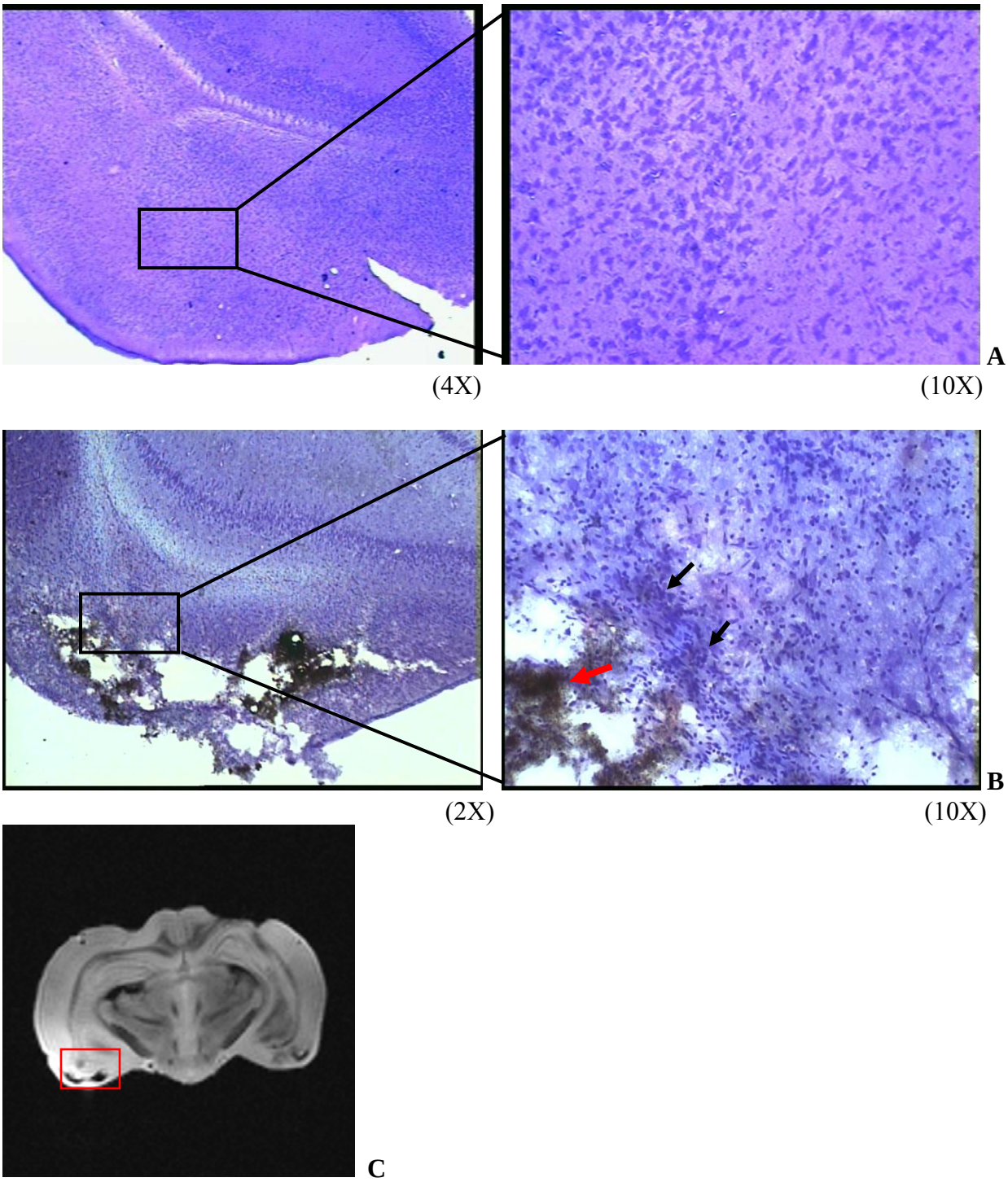

Figure 3-15. Perl's reaction counter-stained with Cresyl-Violet in (A) control (MR Rat 9), and (B) epileptic brain. The epileptic brain shows cavitation in the piriform cortex bilaterally with iron deposition (red arrow), as well as aggregation of microglia (black arrows) around the cavities at high magnification. (C) T2-weighted *ex vivo* MR scan showing piriform cortex region of interest.

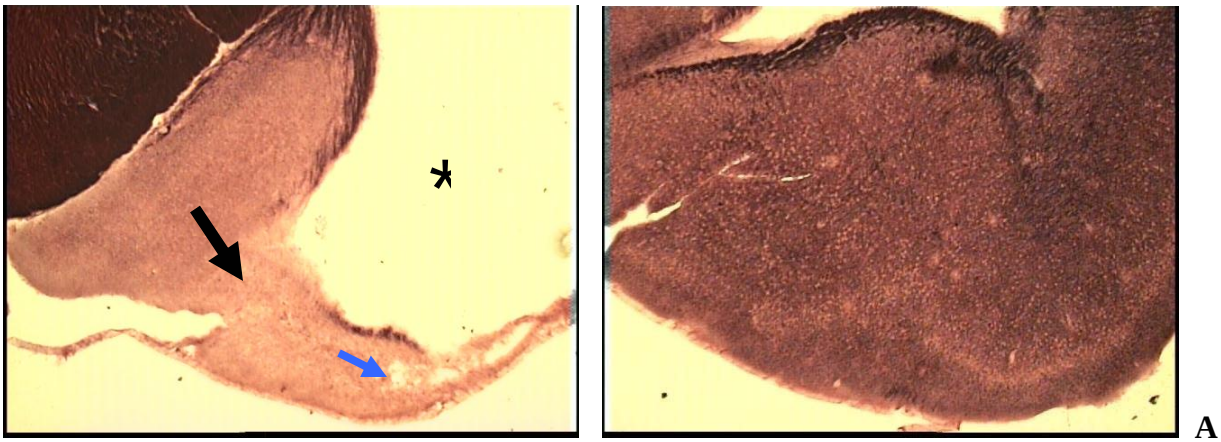

60 days after SE **(4X)** **Control** **(4X)** **A**

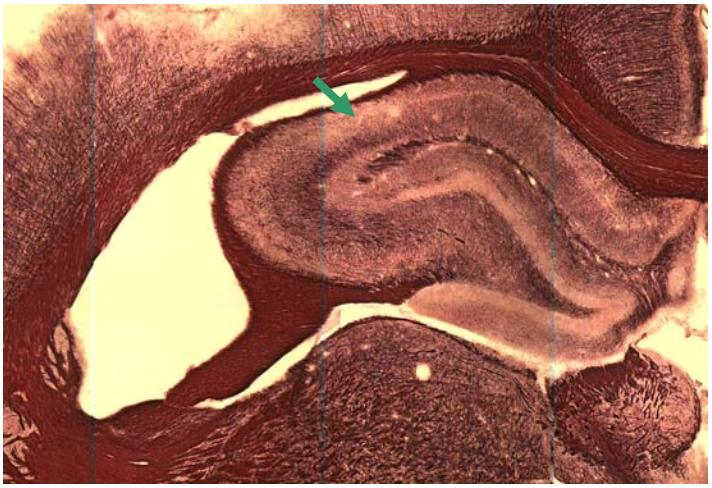

B

(4X)

Figure 3-16. Sections stained for myelin with Black Gold show (A) loss of myelin staining in the amygdala (black arrow). Note also the enlargement of the ventricles (star), secondary to loss of tissue and cavitation in the amygdala and piriform cortex (blue arrow). (B) The CA1 subfield of the hippocampus (green arrow) also lacked myelin staining.

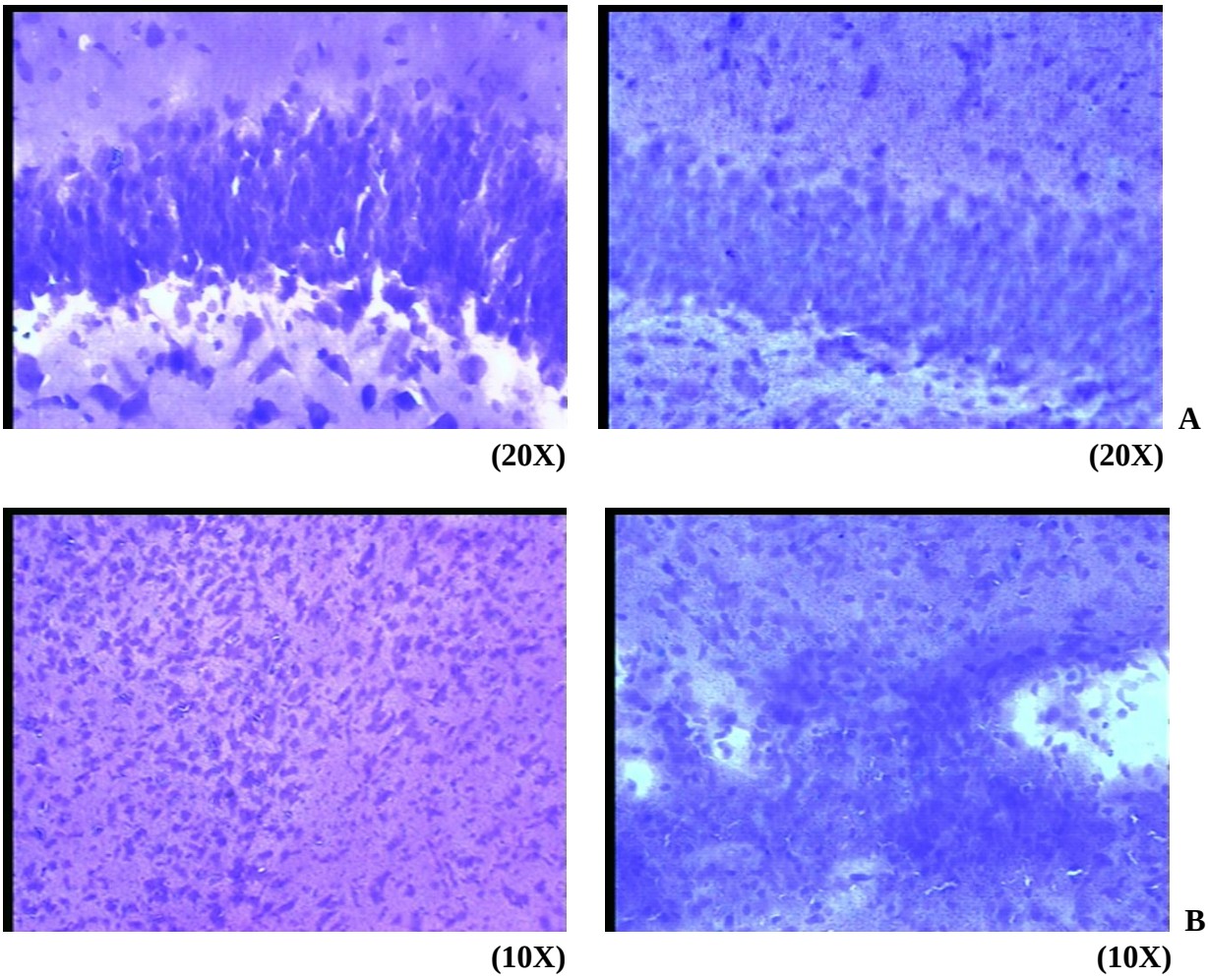

Figure 3-17. Perl sections counter-stained with Cresyl-Violet in animal sacrificed day 9 after SE (MR Rat 14, right). (A) granule cell layer of dentate gyrus showing diffuse iron desposition in SE animal, (B) piriform cortex showing cavitation and microglia aggregation (dark blue cells), compared to control (MR Rat 9, left).

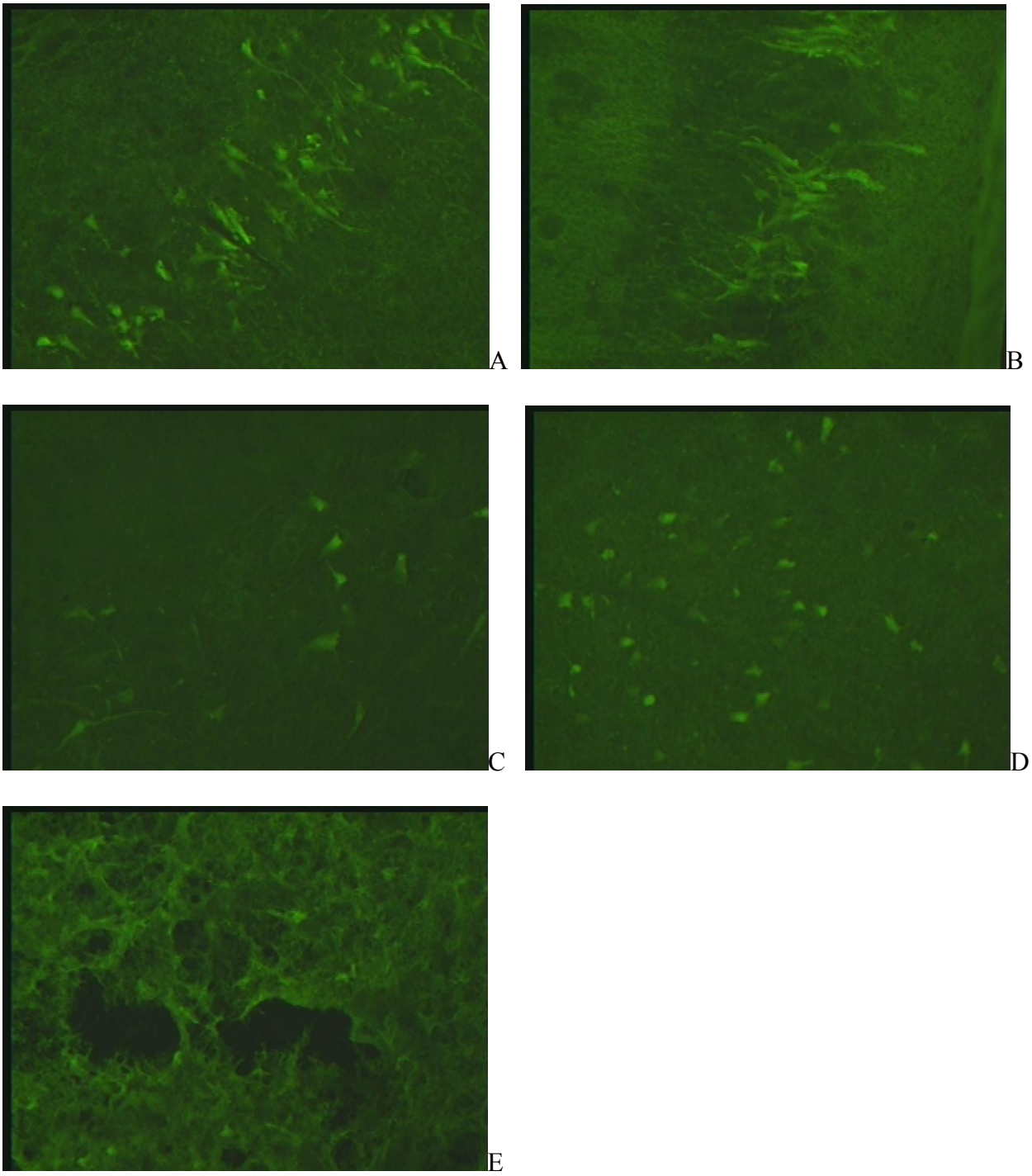

Figure 3-18. Fluoro-Jade C section of one epileptic brain sacrificed 9 days after SE (MR Rat 14) shows the presence of ongoing degenerating neurons in (A) the CA1 pyramidal cell layer, (B) CA3, (C) dentate hilus of the hippocampus, (D) thalamus and (E) piriform cortex. Neurons undergoing degeneration appear fluorescent green compared to the background. These areas showed significant T2 increase between 3 and 10 days after SE.

CHAPTER 4
DISCUSSION

Clinically, MR imaging has been useful in diagnosing the various types of epilepsy and detecting the secondary complications associated with seizures (Bernasconi, et al. 2005, Duncan 1997, Kimiwada, et al. 2006, Wieshmann 2003). In animal research, the CLE model has been shown to produce pathophysiologic changes similar to those observed in human MTLE. Considering the lack of understanding of the causes and mechanisms leading to the recurrence of spontaneous seizures in this common type of drug-refractory epilepsy, it may be possible to gain insight into the mechanisms of epileptogenesis by using *in vivo* MR imaging.

As of now, it is not possible to study the evolution of damage from SE until the occurrence of spontaneous seizures in a single animal with a technique other than MRI. Continued research is needed to enhance this technique and expand its uses to provide a better understanding of the mechanisms responsible for the pathologic changes associated with MTLE. For instance, an important question related to MTLE is the temporal profile of pathologic changes following SE. Using *in vivo* MR imaging, it is possible to monitor these changes in the same animal over time. In the present study, a combination of *in vivo*, *ex vivo* and histological methods was used to study an experimental model of MTLE.

This is the first longitudinal imaging study using an animal model of MTLE with electrical stimulation in the hippocampus inducing SE, followed by a latent period before the appearance of spontaneous seizures (Bertram and Cornett 1994). The findings demonstrated that development of seizures was associated with significant changes in relaxation measurements following electrically induced SE, visible or not as signal intensity changes on T1 or T2-weighted *in vivo* MRI images. These *in vivo* changes were due to underlying pathological tissue alterations evident with *ex vivo* MRI and histology.

Significant changes in relaxation measurements were present three days after SE in the hippocampus, lateral ventricles, amygdala and piriform cortex (PC) regions. T2 relaxation measurements changed more significantly than T1 values in these regions. However, no signal changes in intensity were apparent on T1 or T2-weighted scans in the hippocampus. The dorsal thalamus showed significant changes in relaxation times later during the process, once spontaneous seizures had begun. These results show that limbic structures, as well as the dorsal thalamic areas, play a critical role in epileptogenesis.

The T2 signal is dependent on the relationship between bound and free water in tissue, which is dependent on the macromolecular environment. Disruption in tissue integrity can result in increased free water in tissue and increased in T2 relaxation time. Changes in T2 in the brain have been related to pathological processes like gliosis, demyelination, edema and neuronal loss (Armstrong 1993, Eriksson, et al. 2007, Petropoulos, et al. 2006). Those underlying pathological processes were assessed by histological analysis following MR imaging.

Here we could demonstrate that the first structures injured after SE were the PC, amygdala, lateral ventricles, hippocampus and thalamus. Increased *in vivo* T1 and T2 measurements in the lateral ventricle/ fimbriae areas correlated with an enlargement of the ventricles. This enlargement was probably due to atrophy of the hippocampus and the piriform cortex/ amygdala regions visible on *ex vivo* MR images and histology sections (Wolf, et al. 2002). Decreased relaxation time measurements in the hippocampus might be due to neuronal loss, gliosis and iron deposition observable in our histological results and described as hippocampal sclerosis in previous studies (Briellmann, et al. 2002, Fuerst, et al. 2003, Lewis 2005). Whereas MRI changes in the hippocampus, amygdala and lateral ventricles have been widely described in

animal and human epilepsy research studies in the past, these do not emphasize changes in the PC and thalamus.

The PC showed an initial increase in *in vivo* T1 and T2 values which peaked at 3 days after SE and normalized by 10 days, before the appearance of spontaneous seizures, followed by a significant decrease between 20 and 60 days, and significantly lower T1 and T2 values with *ex vivo* MRI. Histological analysis revealed neuronal loss resulting in cavitation bilaterally, as well as abnormal presence of microglia, as early as 9 days after SE. These structural changes were even more severe in epileptic animals at 60 days after SE, with strong iron deposition and microglia aggregation around the cavities. These results correlate with previous studies that have shown significant neuronal loss and glial infiltration in the PC of pilocarpine-treated rats as early as one week after SE (Bertram and Cornett 1994, Chen, et al. 2007, Druga, et al. 2003).

Recently, significant decreases in the numbers of pyramidal cells and interneurons in all layers of all parts of the PC were found in animals stimulated in the ventral hippocampus (Bolkvadze, et al. 2006). Several neurochemical studies have suggested that the PC is critically involved in the process of epileptogenesis. The PC contains the most susceptible neural circuits of all forebrain regions for electrical (or chemical) induction of limbic seizures (Loscher and Ebert 1996). During electrical stimulation of other limbic brain regions, large afterdischarges can be observed in the ipsilateral PC, indicating that the PC is activated early during the kindling process. The interictal discharge originates in the PC, independent of which structure serves as the kindled focus (McIntyre and Kelly 2000). The PC is the most sensitive brain structure to brain damage by continuous or frequent stimulation of the amygdala or hippocampus. Amygdala kindling leads to a circumscribed loss of inhibitory GABA-immunoreactive neurons in the ipsilateral PC, which is likely to explain the increase in excitability of PC pyramidal neurons

during kindling (Lehmann and Löscher 1998). Kindling of the amygdala or hippocampus induces astrogliosis in the PC, indicating neuronal death in this brain region. Furthermore, activation of microglia is seen in the PC after amygdala kindling (Khurgel and Ivy 1996, Khurgel, et al. 1995).

The decrease in relaxation time values observed 10 days after SE in our study correlates with the neuronal loss and probable gliosis reported in our histological results and previous research studies. The initial increase in relaxation times peaking at day 3 after SE can probably be attributed to edema preceding neuronal loss and gliosis in the amygdalo-piriform region (Briellmann, et al. 2005, Meierkord, et al. 1997, Roch, et al. 2002). For the first time in this CLE model of MTLE, the pathological processes in the piriform cortex could be followed with *in vivo* MRI, in the same animal, from SE to the appearance of spontaneous seizures, confirming the important role of high resolution *in vivo* MRI in studying the progression of epilepsy.

This study has also shown strong iron deposition in the dorsal thalamic nuclei in animals undergoing SE and subsequent chronic seizures. Iron deposition in the thalamus was observed as early as 9 days after stimulation after histological analysis. These iron deposits were seen as areas of decreased T2 and T1 measurements on MRI in our results as well as previous studies (Brittenham and Badman 2003, Clement, et al. 2007, Michaeli, et al. 2007, Neema, et al. 2007), due to the paramagnetic nature of iron particles. In addition to the limbic structures involved in the excitatory circuit of the entorhinal- hippocampal loop (Lothman, et al. 1991, Pare, et al. 1992, Rafiq, et al. 1993), subcortical changes have been described in patients (Sperling, et al. 1990) and animal models (Clifford, et al. 1987), suggesting that limbic epilepsy can be viewed as a disorder of the limbic system as a whole with involvement of extra limbic structures (Bertram 1997, Bertram and Cornett 1994).

In particular, several studies have suggested the midline thalamus to be importantly involved in seizure activity. Tract tracing has shown reciprocal connections between the thalamus and limbic structures (DollemanVanderWeel and Witter 1996, Wouterlood, et al. 1990). Other studies demonstrate that the thalamic nuclei have an excitatory effect on the hippocampus (Bertram and Scott 2000, Dolleman-Van der Weel, et al. 1997). These nuclei also undergo specific pathologic changes in temporal epilepsy (Clifford, Olney, Maniotis, Collins and Zorumski 1987), especially in the medial dorsal thalamus (Juhasz, et al. 1999). In an animal model of chronic limbic epilepsy stimulated in the hippocampus, the seizure onset in the thalamus was linked to seizure onset in the hippocampus; there was also consistent neuronal loss in the midline thalamus similar to neuronal loss and atrophy seen in hippocampal sclerosis (Bertram, et al. 2001, Druga, et al. 2005). Significant changes in the physiology of the medial dorsal thalamic neurons from epileptic rats resulted in hyperexcitability, and inhibition of neuronal activity in the midline thalamus could reduce seizure activity in the hippocampus Khurgel, et al. 1995). These changes were not observed after multiple kindled seizures, which suggests that those changes in the midline thalamus are involved in the genesis of chronic epilepsy and are not a consequence of induced seizures.

In our study, the presence of iron deposits in the dorsal thalamic nuclei suggests neuronal or microglial degeneration, which might take place as early as 9 days after SE, according to our histological data. Iron-mediated oxidative stress has been widely described in neurodegenerative diseases (Shoham 2001; Berg 2006; Brass 2006 (see other ref.); Stankiewicz 2007). It is not clear whether iron deposition contributes to the pathophysiology or is a result of tissue damage in these neurological disorders or epilepsy, but it has been present in many neurological disorders associated with neuronal degeneration. Iron in the dorsal thalamus, although not observable

visually on T1 or T2-weighted *in vivo* MR images, was detectable by a significant decrease in T2 relaxation time *in vivo* after 10 days post-SE. High resolution MRI at 17.6 T revealed areas of hypointensities and decreased T2 values in the dorsal thalamic region bilaterally, which were correlated with iron deposition after histological analysis. This deposition of iron in the thalamus detectable with MRI techniques, suggestive of neuronal degeneration, has not yet been reported in previous epilepsy studies.

In conclusion, we identified biologically relevant correlations between variations in MR relaxation time measurements and pathological changes occurring during epileptogenesis and spontaneous seizures. For instance, an increase in T2 relaxation time correlated with increased ventricular volume, associated with atrophy of the hippocampus and the PC/ amygdala regions in the brains of epileptic animals. Decreased T2 relaxation time was correlated with neuronal loss, gliosis and iron deposition in the dorsal thalamus and the hippocampus, particularly in the dentate gyrus and CA1 subregions. These *in vivo* MR changes were detected after quantification of relaxation times, but not always visible as signal intensity changes on *in vivo* images.

Even though *in vivo* MRI was necessary for the longitudinal observation of the progression of the disease in the same animal, high resolution MR microscopy and histology allowed for a more accurate determination of underlying pathological changes. In order to obtain satisfactory signal- to- noise ratios with *in vivo* imaging, many averages have to be acquired, and scan times are very long, raising the problem of motion artifacts. *Ex vivo* MR imaging does not suffer from these drawbacks and higher spatial resolution, signal-to-noise ratio and sensitivity can be obtained with long acquisition times without trouble. Clinically, newer MRI methods with higher field strength, improved signal-to-noise ratios and newer sequences could detect cerebral

abnormalities not identified on routine imaging in epileptic patients whose optimal MRI is said to be “normal.”

LIST OF REFERENCES

Aliashkevich AF, Yilmazer-Hanke D, Van Roost D, Mundhenk B, Schramm J, Blumcke I. (2003) Cellular pathology of amygdala neurons in human temporal lobe epilepsy. *Acta Neuropathologica* 106:99-106.

Armstrong DD. (1993) The neuropathology of temporal lobe epilepsy. *J Neuropathol Exp Neurol* 52:433-443.

Babb TL, Kupfer WR, Pretorius JK, Crandall PH, Levesque MF. (1991) Synaptic reorganization by mossy fibers in human epileptic fascia dentata. *Neuroscience* 42:351-363.

Bartolomei F, Khalil M, Wendling F, Sontheimer A, Regis J, Ranjeva JP, Guye M, Chauvel P. (2005) Entorhinal cortex involvement in human mesial temporal lobe epilepsy: an electrophysiologic and volumetric study. *Epilepsia* 46:677-687.

Bartolomei F, Wendling F, Bellanger J-J, Regis J, Chauvel P. (2001) Neural networks involving the medial temporal structures in temporal lobe epilepsy. *Clinical Neurophysiology* 112:1746-1760.

Berg AT, Levy SR, Testa FM, Shinnar S. (1999) Treatment of Newly Diagnosed Pediatric Epilepsy: A Community-Based Study. pp. 1267-1271.

Bernasconi N, Bernasconi A, Andermann F, Dubeau F, Feindel W, Reutens DC. (1999) Entorhinal cortex in temporal lobe epilepsy: a quantitative MRI study. *Neurology* 52:1870-1876.

Bernasconi N, Natsume J, Bernasconi A. (2005) Progression in temporal lobe epilepsy: differential atrophy in mesial temporal structures. *Neurology* 65:223-228.

Bertram EH, Lothman EW, Lenn NJ. (1990) The Hippocampus in Experimental Chronic Epilepsy - a Morphometric Analysis. *Ann Neurol* 27:43-48.

Bertram EH, 3rd, Lothman EW. (1993) Morphometric effects of intermittent kindled seizures and limbic status epilepticus in the dentate gyrus of the rat. *Brain Res* 603:25-31.

Bertram EH, Cornett J. (1993) The ontogeny of seizures in a rat model of limbic epilepsy: evidence for a kindling process in the development of chronic spontaneous seizures. *Brain Res* 625:295-300.

Bertram EH, Cornett JF. (1994) The evolution of a rat model of chronic spontaneous limbic seizures. *Brain Res* 661:157-162.

Bertram EH. (1997) Functional anatomy of spontaneous seizures in a rat model of limbic epilepsy. *Epilepsia* 38:95-105.

Bertram EH, Scott C. (2000) The pathological substrate of limbic epilepsy: neuronal loss in the medial dorsal thalamic nucleus as the consistent change. *Epilepsia* 41 Suppl 6:S3-8.

Bertram EH, Mangan PS, Zhang D, Scott CA, Williamson JM. (2001) The Midline Thalamus: Alterations and a Potential Role in Limbic Epilepsy. pp. 967-978.

Bhagat YA, Obenaus A, Hamilton MG, Kendall EJ. (2001) Magnetic resonance imaging predicts neuropathology from soman-mediated seizures in the rodent. *NeuroReport* 12:1481-1487.

Blumcke I, Beck H, Lie AA, Wiestler OD. (1999) Molecular neuropathology of human mesial temporal lobe epilepsy. *Epilepsy Res Suppl* 36:205-223.

Blumenfeld H, McNally KA, Vanderhill SD, Paige AL, Chung R, Davis K, Norden AD, Stokking R, Studholme C, Novotny EJ, Zubal IG, Spencer SS. (2004) Positive and negative network correlations in temporal lobe epilepsy. *Cerebral Cortex* 14:892-902.

Bolkvadze T, Dzhaparidze N, Zhvaniya M, Kotariya N, Tsitsishvili A. (2006) Cellular Composition of the Piriform Cortex of the Rat Brain in Experimental Epilepsy. *Neuroscience and Behavioral Physiology* 36:271-274.

Bouilleret V, Nehlig A, Marescaux C, Namer IJ. (2000) Magnetic resonance imaging follow-up of progressive hippocampal changes in a mouse model of mesial temporal lobe epilepsy. *Epilepsia* 41:642-650.

Briellmann RS, Kalnins RM, Berkovic SF, Jackson GD. (2002) Hippocampal pathology in refractory temporal lobe epilepsy: T2-weighted signal change reflects dentate gliosis. *Neurology* 58:265-271.

Briellmann RS, Wellard RM, Jackson GD. (2005) Seizure-associated abnormalities in epilepsy: evidence from MR imaging. *Epilepsia* 46:760-766.

Brittenham GM, Badman DG. (2003) Noninvasive measurement of iron: report of an NIDDK workshop. *Blood* 101:15-19.

Brooks-Kayal AR, Shumate MD, Jin H, Rikhter TY, Coulter DA. (1998) Selective changes in single cell GABAA receptor subunit expression and function in temporal lobe epilepsy. *Nat Med* 4:1166-1172.

Buhl EH, Otis TS, Mody I. (1996) Zinc-induced collapse of augmented inhibition by GABA in a temporal lobe epilepsy model. *Science* 271:369-373.

Buser P, Bancaud J. (1983) Unilateral connections between amygdala and hippocampus in man. A study of epileptic patients with depth electrodes. *Electroencephalogr Clin Neurophysiol* 55:1-12.

Cavazos JE, Cross DJ. (2006) The role of synaptic reorganization in mesial temporal lobe epilepsy. *Epilepsy Behav* 8:483-493.

Chang BS, Lowenstein DH. (2003) Mechanisms of disease - Epilepsy. *New England Journal of Medicine* 349:1257-1266.

Chen S, Kobayashi M, Honda Y, Kakuta S, Sato F, Kishi K. (2007) Preferential neuron loss in the rat piriform cortex following pilocarpine-induced status epilepticus. *Epilepsy Res Suppl* 74:1-18.

Clement F, Devos D, Moreau C, Coubes P, Destee A, Defebvre L. (2007) Neurodegeneration with brain iron accumulation: clinical, radiographic and genetic heterogeneity and corresponding therapeutic options. *Acta Neurol Belg* 107:26-31.

Clifford DB, Olney JW, Maniotis A, Collins RC, Zorumski CF. (1987) The functional anatomy and pathology of lithium-pilocarpine and high-dose pilocarpine seizures. *Neuroscience* 23:953-968.

Cossart R, Dinocourt C, Hirsch JC, Merchan-Perez A, De Felipe J, Ben-Ari Y, Esclapez M, Bernard C. (2001) Dendritic but not somatic GABAergic inhibition is decreased in experimental epilepsy. *Nat Neurosci* 4:52-62.

Dolleman-Van der Weel MJ, Lopes da Silva FH, Witter MP. (1997) Nucleus Reuniens Thalami Modulates Activity in Hippocampal Field CA1 through Excitatory and Inhibitory Mechanisms. pp. 5640-5650.

DollemanVanderWeel MJ, Witter MP. (1996) Projections from the nucleus reuniens thalami to the entorhinal cortex, hippocampal field CA1, and the subiculum in the rat arise from different populations of neurons. *Journal of Comparative Neurology* 364:637-650.

Druga R, Kubova H, Suchomelova L, Haugvicova R. (2003) Lithium/pilocarpine status epilepticus-induced neuropathology of piriform cortex and adjoining structures in rats is age-dependent. *Physiological Research* 52:251-264.

Druga R, Mares P, Otahal J, Kubova H. (2005) Degenerative neuronal changes in the rat thalamus induced by status epilepticus at different developmental stages. *Epilepsy Res Suppl* 63:43-65.

Du F, Whetsell WO, Abou-Khalil B, Blumenkopf B, Lothman EW, Schwarcz R. (1993) Preferential neuronal loss in layer III of the entorhinal cortex in patients with temporal lobe epilepsy. *Epilepsy Res Suppl* 16:223-233.

Dube C, Yu H, Nalcioglu O, Baram TZ. (2004) Serial MRI after experimental febrile seizures: altered T2 signal without neuronal death. *Ann.Neurol.* 56:709-714.

Duncan JS. (1997) Imaging and epilepsy. *Brain* 120 (Pt 2):339-377.

Engel J, Jr. (2001) Mesial Temporal Lobe Epilepsy: What Have We Learned? 7:340-352.

Engelhorn T, Weise J, Hammen T, Bluemcke I, Hufnagel A, Doerfler A. (2007) Early diffusion-weighted MRI predicts regional neuronal damage in generalized status epilepticus in rats treated with diazepam. *Neurosci Lett* 417:275-280.

Eriksson SH, Free SL, Thom M, Martinian L, Symms MR, Salmenpera TM, McEvoy AW, Harkness W, Duncan JS, Sisodiya SM. (2007) Correlation of quantitative MRI and neuropathology in epilepsy surgical resection specimens--T2 correlates with neuronal tissue in gray matter. *neuroimage* 37:48-55.

Fuerst D, Shah J, Shah A, Watson C. (2003) Hippocampal sclerosis is a progressive disorder: a longitudinal volumetric MRI study. *Ann.Neurol.* 53:413-416.

Gloor P. (1997) *The Temporal Lobe and Limbic System*. Oxford University Press, Oxford.

Goncalves PPM, Insausti R, Artacho-Perula E, Salmenpera T, Kalviainen R, Pitkanen A. (2005) MR volumetric analysis of the piriform cortex and cortical amygdala in drug-refractory temporal lobe epilepsy. *ANJR Am J Neuroradiol.* 26:319-332.

Guilfoyle DN, Helpern JA, Lim KO. (2003) Diffusion tensor imaging in fixed brain tissue at 7.0 T. *NMR Biomed* 16:77-81.

Hudson LP, Munoz DG, Miller L, McLachlan RS, Girvin JP, Blume WT. (1993) Amygdaloid sclerosis in temporal lobe epilepsy. pp. 622-631.

Jackson G, McIntosh A, Briellmann R, Berkovic S. (1998) Hippocampal sclerosis studied in identical twins. *Neurology* 51:78–84.

Juhasz C, Nagy F, Watson C, da Silva EA, Muzik O, Chugani DC, Shah J, Chugani HT. (1999) Glucose and [11C]flumazenil positron emission tomography abnormalities of thalamic nuclei in temporal lobe epilepsy. pp. 2037-40.

Jupp B, Williams JP, Tesiram YA, Vosmansky M, O'Brien TJ. (2006) Hippocampal T2 signal change during amygdala kindling epileptogenesis. *Epilepsia* 47:41-46.

Khurgel M, Ivy GO. (1996) Astrocytes in kindling: Relevance to epileptogenesis. *Epilepsy Res Suppl* 26:163-175.

Khurgel M, Switzer RC, Teskey GC, Spiller AE, Racine RJ, Ivy GO. (1995) Activation of Astrocytes During Epileptogenesis in the Absence of Neuronal Degeneration. *Neurobiol Dis* 2:23-35.

Kimiwada T, Juhasz C, Makki M, Muzik O, Chugani DC, Asano E, Chugani HT. (2006) Hippocampal and thalamic diffusion abnormalities in children with temporal lobe epilepsy. *Epilepsia* 47:167-175.

Kemppainen S, Jolkkonen E, Pitkanen A. (2002) Projections from the posterior cortical nucleus of the amygdala to the hippocampal formation and parahippocampal region in rat. *Hippocampus* 12:735-755.

Kemppainen S, Pitkanen A. (2004) Damage to the amygdalo-hippocampal projection in temporal lobe epilepsy: a tract-tracing study in chronic epileptic rats. *Neuroscience* 126:485-501.

King M, Bruggen NV, Ahier RG, Cremer JE, Hajnal JV, Doran SRWM. (1991a) Diffusion-weighted imaging of kainic acid lesions in the rat brain 20:158-164.

King MD, Vanbruggen N, Ahier RG, Cremer JE, Hajnal JV, Williams SR, Doran M. (1991b) DIFFUSION-WEIGHTED IMAGING OF KAINIC ACID LESIONS IN THE RAT-BRAIN. *Magnetic Resonance in Medicine* 20:158-164.

Knudsen FU, Auk I. (2000) Clinical audit in the management of children with epilepsy. pp. 502-504.

Lehmann H, Löscher UEW. (1998) Amygdala-kindling induces a lasting reduction of GABA-immunoreactive neurons in a discrete area of the ipsilateral piriform cortex 29:299-309.

Lemaire C, Duncan EG, Solsberg MD, Armstrong RL. (1990) In vitro magnetic resonance microimaging of the spinal cord. *Magn.Reson.Med.* 14:97-104.

Lewis DV. (2005) Losing neurons: selective vulnerability and mesial temporal sclerosis. *Epilepsia* 46 Suppl 7:39-44.

Liu Z, Mikati M, Holmes GL. (1995) Mesial Temporal Sclerosis - Pathogenesis and Significance. *Pediatric Neurology* 12:5-16.

Loscher W, Ebert U. (1996) The role of the piriform cortex in kindling. *Progress in Neurobiology* 50:427-481.

Lothman EW, Bertram EH, Bekenstein JW, Perlin JB. (1989) Self-sustaining limbic status epilepticus induced by 'continuous' hippocampal stimulation: electrographic and behavioral characteristics. *Epilepsy Res* 3:107-119.

Lothman EW, Bertram EH, Kapur J, Stringer JL. (1990) Recurrent Spontaneous Hippocampal Seizures in the Rat as a Chronic Sequela to Limbic Status Epilepticus. *Epilepsy Res Suppl* 6:110-118.

Lothman EW, Bertram EH, Stringer JL. (1991) Functional anatomy of hippocampal seizures. *Progress in Neurobiology* 37:1-82.

Maillard L, Vignal J-P, Gavaret M, Guye M, Biraben A, McGonigal A, Chauvel P, Bartolomei F. (2004) Semiologic and Electrophysiologic Correlations in Temporal Lobe Seizure Subtypes. pp. 1590-1599.

Mathern GW, Babb TL, Leite JP, Pretorius JK, Yeoman KM, Kuhlman PA. (1996) The pathogenic and progressive features of chronic human hippocampal epilepsy. *Epilepsy Res Suppl* 26:151-161.

Mathern GW, Bertram EH, 3rd, Babb TL, Pretorius JK, Kuhlman PA, Spradlin S, Mendoza D. (1997) In contrast to kindled seizures, the frequency of spontaneous epilepsy in the limbic status model correlates with greater aberrant fascia dentata excitatory and inhibitory axon sprouting, and increased staining for N-methyl-D-aspartate, AMPA and GABA(A) receptors. *Neuroscience* 77:1003-1019.

McIntyre DC, Kelly ME. (2000) The Parahippocampal Cortices and Kindling. pp. 343-354.

Meierkord H, Wieshmann U, Niehaus L, Lehmann R. (1997) Structural consequences of status epilepticus demonstrated with serial magnetic resonance imaging. *Acta Neurol.Scand.* 96:127-132.

Michaeli S, Oz G, Sorce DJ, Garwood M, Ugurbil K, Majestic S, Tuite P. (2007) Assessment of brain iron and neuronal integrity in patients with Parkinson's disease using novel MRI contrasts. *Movement Disorders* 22:334-340.

Nairismagi J, Grohn OH, Kettunen MI, Nissinen J, Kauppinen RA, Pitkanen A. (2004) Progression of brain damage after status epilepticus and its association with epileptogenesis: a quantitative MRI study in a rat model of temporal lobe epilepsy. *Epilepsia* 45:1024-1034.

Neema M, Stankiewicz J, Arora A, Dandamudi VSR, Batt CE, Guss ZD, Al-Sabbagh A, Bakshi R. (2007) T1-and T2-based MRI measures of diffuse gray matter and white matter damage in patients with multiple sclerosis. *Journal of Neuroimaging* 17:16S-21S.

Niessen HG, Angenstein F, Vielhaber S, Frisch C, Kudin A, Elger CE, Heinze HJ, Scheich H, Kunz WS. (2005) Volumetric magnetic resonance imaging of functionally relevant structural alterations in chronic epilepsy after pilocarpine-induced status epilepticus in rats. *Epilepsia* 46:1021-1026.

Pare D, deCurtis M, Llinas R. (1992) Role of the hippocampal-entorhinal loop in temporal lobe epilepsy: extra- and intracellular study in the isolated guinea pig brain in vitro. pp. 1867-1881.

Parent JM, Yu TW, Leibowitz RT, Geschwind DH, Sloviter RS, Lowenstein DH. (1997) Dentate Granule Cell Neurogenesis Is Increased by Seizures and Contributes to Aberrant Network Reorganization in the Adult Rat Hippocampus. pp. 3727-3738.

Petropoulos H, Friedman SD, Shaw DWW, Artru AA, Dawson G, Dager SR. (2006) Gray matter abnormalities in autism spectrum disorder revealed by T2 relaxation. *Neurology* 67:632-636.

Pikkarainen M, Ronkko S, Savander V, Insausti R, Pitkanen A. (1999) Projections from the lateral, basal, and accessory basal nuclei of the amygdala to the hippocampal formation in rat. *Journal of Comparative Neurology* 403:229-260.

Pitkanen A, Nissinen J, Nairismagi J, Lukasiuk K, Grohn OH, Miettinen R, Kauppinen R. (2002) Progression of neuronal damage after status epilepticus and during spontaneous seizures in a rat model of temporal lobe epilepsy. *Prog.Brain Res.* 135:67-83.

Rafiq A, DeLorenzo RJ, Coulter DA. (1993) Generation and propagation of epileptiform discharges in a combined entorhinal cortex/hippocampal slice. pp. 1962-1974.

Roch C, Leroy C, Nehlig A, Namer IJ. (2002) Magnetic resonance imaging in the study of the lithium-pilocarpine model of temporal lobe epilepsy in adult rats. *Epilepsia* 43:325-335.

Roch C, Leroy C, Nehlig A, Namer IJ. (2002b) Predictive value of cortical injury for the development of temporal lobe epilepsy in 21-day-old rats: an MRI approach using the lithium-pilocarpine model. *Epilepsia* 43:1129-1136.

Sander JW. (2003) The epidemiology of epilepsy revisited. *Curr Opin Neurol* 16:165-170.

Scharfman HE, Goodman JH, Sollas AL. (2000) Granule-Like Neurons at the Hilar/CA3 Border after Status Epilepticus and Their Synchrony with Area CA3 Pyramidal Cells: Functional Implications of Seizure-Induced Neurogenesis. pp. 6144-6158.

Sloviter R. (1991) Permanently altered hippocampal structure, excitability, and inhibition after experimental status epilepticus in the rat: The ?dormant basket cell? hypothesis and its possible relevance to temporal lobe epilepsy 1:41-66.

Soltesz I. (1995) Brief history of cortico-hippocampal time with a special reference to the direct entorhinal input to CA1. *Hippocampus* 5:120-124.

Sperling MR, Gur RC, Alavi A, Gur RE, Resnick S, Oconnor MJ, Reivich M. (1990) Subcortical Metabolic Alterations in Partial Epilepsy. *Epilepsia* 31:145-155.

Sundqvist A. (2002) Epilepsy: a clinical diagnostic overview. *European Journal of Pain* 6:21-25.

Sutula T, Cascino G, Cavazos J, Parada I, Ramirez L. (1989) Mossy fiber synaptic reorganization in the epileptic human temporal lobe. pp. 321-330.

Tiina-Riikka M, Pitkänen A, Tuunanen J, Kauppinen RA. (2001) Ex vivo MR microimaging of neuronal damage after kainate-induced status epilepticus in rat: Correlation with quantitative histology. pp. 946-954.

Tuunanen J, Lukasiuk K, Halonen T, Pitkanen A. (1999) Status epilepticus-induced neuronal damage in the rat amygdaloid complex: distribution, time-course and mechanisms. *Neuroscience* 94:473-495.

van Eijsden P, Notenboom RG, Wu O, de Graan PN, van Nieuwenhuizen O, Nicolay K, Braun KP. (2004) In vivo 1H magnetic resonance spectroscopy, T2-weighted and diffusion-weighted MRI during lithium-pilocarpine-induced status epilepticus in the rat. *Brain Res.* 1030:11-18.

von Bohlen und H, Schulze K, Albrecht D. (2004) Amygdala-kindling induces alterations in neuronal density and in density of degenerated fibers. *Hippocampus* 14:311-318.

Wall CJ, Kendall EJ, Obenaus A. (2000) Rapid alterations in diffusion-weighted images with anatomic correlates in a rodent model of status epilepticus. *AJNR Am.J.Neuroradiol.* 21:1841-1852.

Wang Y, Majors A, Najm I, Xue M, Comair Y, Modic M, Ng TC. (1996) Postictal alteration of sodium content and apparent diffusion coefficient in epileptic rat brain induced by kainic acid. *Epilepsia* 37:1000-1006.

Wieshmann UC. (2003) Clinical application of neuroimaging in epilepsy. *J Neurol Neurosurg Psychiatry* 74:466-470.

Wilson CL, Isokawa M, Babb TL, Crandall PH. (1990) Functional Connections in the Human Temporal-Lobe .1. Analysis of Limbic System Pathways Using Neuronal Responses Evoked by Electrical-Stimulation. *Experimental Brain Research* 82:279-292.

Wolf OT, Dyakin V, Patel A, Vadasz C, de Leon MJ, McEwen BS, Bulloch K. (2002) Volumetric structural magnetic resonance imaging (MRI) of the rat hippocampus following kainic acid (KA) treatment. *Brain Res.* 934:87-96.

Wouterlood FG, Boon ME, Kok LP. (1990) Immunocytochemistry on Free-Floating Sections of Rat-Brain Using Microwave Irradiation During the Incubation in the Primary Antiserum - Light and Electron-Microscopy. *Journal of Neuroscience Methods* 35:133-145.

BIOGRAPHICAL SKETCH

Lan Hoang Minh was born and grew up in Paris, France, in 1978. After graduating from high school baccalaureate with honors in 1996, Lan worked for one year as a administrative assistant for a medical clinic, before coming to the United States to attend the undergraduate program at the University of Florida, in the hope of integrating medical school after college. During her undergraduate education, she also gained valuable research experience as a UF Undergraduate Research Scholar in the microbiology laboratory of Dr. Kenneth Rand at Shands Hospital. Lan graduated with a Bachelor of Science in microbiology in 2001 and entered the College of Medicine program at the University of Florida that Fall. After a couple of years in medical school, she joined the Biomedical Engineering program that she deemed suited more her interests. She joined the laboratory of Dr. Thomas Mareci, in collaboration with Dr. Paul Carney's lab, in studying evolution into epilepsy using magnetic resonance imaging.